frontiers | Frontiers in Marine Science

TYPE Original Research
PUBLISHED 07 April 2025
DOI 10.3389/fmars.2025.1534727

EDITED BY
Zhongxian Zhao,
Chinese Academy of Sciences (CAS), China

REVIEWED BY
Jiangbo Ren,
Guangzhou Marine Geological Survey, China
Yanhui Dong,
Ministry of Natural Resources, China

*CORRESPONDENCE
Xiaoyu Zhang
zhang_xiaoyu@zju.edu.cn

RECEIVED 26 November 2024
ACCEPTED 11 February 2025
PUBLISHED 07 April 2025

CITATION
Xu Z, Zhang X, Zhu K, Huang M, Yu M, Li Z, Qiu Z and Lu Y (2025) Comparison of elemental composition and $^{87}Sr/^{86}Sr$-$^{143}Nd/^{144}Nd$ between fossil and modern fish teeth and the significance of the enrichment of REE in deep-sea sediments. *Front. Mar. Sci.* 12:1534727.
doi: 10.3389/fmars.2025.1534727

Comparison of elemental composition and $^{87}Sr/^{86}Sr$-$^{143}Nd/^{144}Nd$ between fossil and modern fish teeth and the significance of the enrichment of REE in deep-sea sediments

Zhijie Xu[1], Xiaoyu Zhang[1,2]*, Kongyang Zhu[1], Mu Huang[3], Miao Yu[3], Zheng Li[1], Zhongrong Qiu[4] and Yanfang Lu[1]

[1]School of Earth Sciences, Zhejiang University, Hangzhou, China, [2]Hainan Institute, Zhejiang University, Sanya, China, [3]Laboratory of Marine Geology and Geophysics, The First Institute of Oceanography, Ministry of Natural Resources (MNR), Qingdao, China, [4]Ocean College, Zhejiang University, Zhoushan, China

Fossil fish teeth are important carriers of rare earth elements (REEs) in deep-sea sediments. Meanwhile, $^{87}Sr/^{86}Sr$-$^{143}Nd/^{144}Nd$ in these fossils have been widely used in paleoceanography. However, when and how REEs enter the fish teeth remains ambiguous, which hinders elucidating the enrichment mechanism of REEs in deep-sea sediments, and the effectiveness of $^{87}Sr/^{86}Sr$-$^{143}Nd/^{144}Nd$ in paleoceanography is doubted. This study examined the contents of REEs, major and trace elements, and $^{87}Sr/^{86}Sr$-$^{143}Nd/^{144}Nd$ in modern fish teeth and in fossil fish teeth from deep-sea sediments. The results indicated that elemental geochemical properties and a redox environment are the main factors controlling their enrichment process in fish teeth. At least three categories of trace elements are classified during two different stages (physiological process of living fish and post-deposition of fossils): (1) elements of Type I mainly belong to IA, IIA, IIIA, IVA, and transition group with active chemical properties, entering into the fish teeth during life; (2) Type II represents elements from the IA, VA, transition elements, and Actinides groups, and are enriched uninterruptedly from the living fish teeth to the post-deposition fossils with variable valences under different redox conditions; (3) Type III are elements accumulated only after deposition under oxidizing or suboxidizing and are members of Lanthanides and rare dispersed elements groups with a large atomic radius and strong chemical activity. The distinctly different enrichment processes of Sr and Nd, $^{87}Sr/^{86}Sr$, and $^{143}Nd/^{144}Nd$ in fossil fish teeth may represent different material sources and should be cautiously employed in paleoceanography. The continuous rehabilitation of $^{87}Sr/^{86}Sr$ in fossil fish teeth after deposition would change the original $^{87}Sr/^{86}Sr$ of seawater recorded near fish teeth but the content of Sr remains unchanged. As for $^{143}Nd/^{144}Nd$, when Nd enters the fossils after deposition, the exchange of 143Nd/144Nd between particles and pore liquid gradually ceases due to the saturation of the isomorphism lattice. $^{143}Nd/^{144}Nd$ of fossil fish teeth may provide more information about deep seawater at the seawater-sediment interface. This study elucidates the enrichment mechanism of REEs in deep-sea sediments and the cautious utilization of $^{87}Sr/^{86}Sr$ and $^{143}Nd/^{144}Nd$ of fossils is a prerequisite.

KEYWORDS

fossil and modern fish teeth, Central Indian Ocean Basin, trace elements enrichment process, $^{87}Sr/^{86}Sr$-$^{143}Nd/^{144}Nd$, geochemical indicative significance, paleoceanography

1 Introduction

As a group of elements with symbiotic properties, rare earth elements (REEs) have been widely used as tracers in different earth systems (Elderfield et al., 1990; Sholkovitz, 1993; Sun et al., 2023; Vanderstraeten et al., 2023; Weng et al., 2023) and have important significance in mineral resources (Nassar et al., 2015). Since the first report of heavily REE-enriched deep-sea sediment in the Pacific (Piper, 1974), deep-sea sediment containing higher than 400 ppm of REEs has been indicated as potential rare earth mineral resources nearly 50 years later (Kato et al., 2011). Subsequent studies have shown that REE-rich deep-sea sediments mainly develop in the Pacific Ocean and Indian Ocean (Kato et al., 2011; Kon et al., 2014; Yasukawa et al., 2014; Tanaka et al., 2020; Ren et al., 2021, 2022; Liao et al., 2022). The biological apatite (mainly referring to fossil fish teeth/bones) in sediments has been proven to be the main host of REEs with the highest content reaching to 22,000 ppm (Ren et al., 2021). Fossil fish teeth/bones with less than 10% content in sediments can contribute at least 69% of REEs in sediments (Lu et al., 2022; Liao et al., 2022), 1–2 orders of magnitude more than other hosts such as Fe-Mn oxyhydroxides, clay, and phillipsite (Wang et al., 2016; Bi et al., 2021; Liao et al., 2022). Therefore, fossil fish teeth/bones have attracted much attention in studies on the REE mineralization process in the deep sea.

Previous studies have shown that the enrichment of REE by biological apatite in sediments mainly occurs near the seawater/sediment interface in the early diagenetic process (Elderfield and Pagett, 1986; Grandjean et al., 1987; Bi et al., 2021; Ren et al., 2021), and is influenced by bottom water such as South Pacific Gyre and Antarctic bottom water (Ohta et al., 2021; Zhang et al., 2023). Nevertheless, it was found that the diffusion coefficient of REEs in fish bones from sediments in the Pacific is 70 mm^2/my (Toyoda and Tokonami, 1990). With such a slow diffusion rate, the hypothesis is that REE directly entered the interior of the fish teeth from seawater during early diagenesis and high concentrations were doubted. Some studies argue that the enrichment of REEs occurs in a relatively longer period after deposition and absorption from pore water during diagenesis may occur (Liao et al., 2019a; Deng et al., 2022). One explanation is that the enrichment of REEs in deep-sea sediments is due to the significant decrease in the amount of REEs imported into seawater through pore water compared with shallow sea sediments, resulting in a large amount of REEs remaining in sediments and eventually being adsorbed by biological apatite (Deng et al., 2022). This process may also be related to the release of some of the initially adsorbed REEs from Ferrum-Manganese (Fe-Mn) minerals into pore water during oxidizing diagenesis (Liao et al., 2019b). In addition, whether clay minerals act as an intermediate in the enrichment process of REEs in biological apatite needs further investigation (Liu et al., 2023).

Being the main host of REEs, fossil fish teeth, which preserve not only neodymium isotopes ($^{143}Nd/^{144}Nd$) but also strontium isotopes ($^{87}Sr/^{86}Sr$) information, have been widely used as reliable indices in paleoceanography, geological events, and isotope stratigraphy (Wright et al., 1987; Ingram, 1995; Martin and Scher, 2004). However, it was indicated that the $^{87}Sr/^{86}Sr$ ratios of fossil fish teeth could change because of teeth recrystallization and exchange with pore fluid Sr^{2+} during burial and diagenesis, leading to older or younger Sr isotopic stratigraphic age (Martin and Scher, 2004). It has also been pointed out that the fidelity of $^{87}Sr/^{86}Sr$ in fish teeth is related to the density of the structure, and fish teeth with dense structure and low Lanthanum (La) content have a relative $^{87}Sr/^{86}Sr$ ratio, indicating that the Sr isotope is exchanged with the pore water when the elements such as La enter the fish tooth in the early diagenesis. However, some fish teeth are resistant to early diagenetic changes due to their dense structure (Wang et al., 2023). Conversely, the Nd absorption capacity of modern fish teeth is extremely low in ppb level, but the content of Nd in fossil fish teeth is three to six orders of magnitude higher than that in living fish teeth (Wright et al., 1984). The increase in Nd after fish teeth deposition coincides with the rapid transition from hydroxyapatite in live fish teeth to hydroxyfluorapatite in fossil fish teeth and the latter facilitate Nd enrichment, which is believed to be the main enrichment mechanism of Nd in fossil fish teeth (Martin and Haley, 2000). In the past, the rapid adsorption of Nd by fossil fish teeth was believed occur when teeth were still in contact with the bottom water, and the adsorption ceased in the burial stage (Martin and Scher, 2004). However, recent research indicated that the $^{143}Nd/^{144}Nd$ in fossil fish teeth is unevenly distributed and varies widely, increasing gradually from the root and middle to the tip of fish teeth (Deng et al., 2022). It was inferred that the Nd isotopic ratio of biological apatite in deep-sea sediments may be changed by the pore water during diagenesis. The reliability of REEs as tracers in the study of deep-sea sediment material sources needs to be further confirmed, and their usage in paleoceanography needs to be reevaluated as well.

To conclude, the enrichment mechanism of REEs in fossil fish teeth in deep-sea sediments has not been clearly elucidated, which results in doubts about the reliability of ^{87}Sr/^{86}Sr-^{143}Nd/^{144}Nd of fossil fish teeth as indices in paleoceanography and impacts the expounding of the material sources of highly enriched REEs in deep-sea sediments. Systematic comparative studies on the geochemical characteristics of these elements and isotopes in modern and fossil fish teeth may be conducive to understanding the enrichment process and influencing factors of these elements and isotopes in fish teeth. In this study, we detect the major and trace elements, REEs, and Sr-Nd isotopes in fossil fish teeth from the Central Indian Ocean Basin (CIOB) and modern fish teeth from the East China Sea (ECS) and the Qiandaohu Lake in eastern China, trying to answer the following three research questions: (1) with the comparison of REEs and other elements contained in living and fossil fish teeth, when and how the different elements enter the fish teeth and/or fossils will be discussed; (2) according to their enrichment process in modern and fossil fish teeth, different categories of elements will be classified according to their geochemical properties; (3) the ^{87}Sr/^{86}Sr-^{143}Nd/^{144}Nd record in fossil fish teeth from the CIOB as a material source tracer will be re-examined to analyze the impacting factors on its reliability when used to in paleoceanography. This study will explore the enrichment mechanism of REEs in deep-sea sediments and the utility of ^{87}Sr/^{86}Sr-^{143}Nd/^{144}Nd of fossils in paleoceanography.

2 Geological background

The locations of the different sampling sites for fossil and modern fish teeth are shown in Figure 1.

2.1 East China Sea

The ECS is one of the largest marginal seas in the Northwest Pacific Ocean. The submarine landform is divided from west to east into the East China Sea shelf, East China Sea slope, Okinawa trough, Kyushu-Ryukyu Island slope, and Ryukyu Island arc (Liu et al., 2003, 2020). The hydrodynamic of the ECS is complex with Changjiang (Yangtze River) diluted water, East China Sea coastal current, Kuroshio, Taiwan Warm Current, and Tsushima warm current (Su, 1998; Zhou et al., 2015). The interaction of these currents has a dominant influence on the regional marine environment. Seasonal changes in different water masses and the mixing of riverine runoff and coastal currents with the intrusion of saline currents significantly affect the redox conditions of the ECS (Sun et al., 2017, 2019). Generally, the strong oxidizing seawater distributes discontinuously in the ECS, in contrast to the weak oxidizing condition of the aquatic environment in spring. Two anoxic zones located at the north and the south Yangtze River estuary are developing, particularly in the summer, and can even merge into one large anoxic zone, which endangers both fish and benthos (Wei et al., 2015).

2.2 Qiandaohu Lake

Qiandaohu Lake is located in eastern China and is fed from the East China Sea, in the low reach of the Changjiang River Basin. There are nearly 30 tributaries entering the lake, among them, Xin'an River is the largest water inflow, accounting for

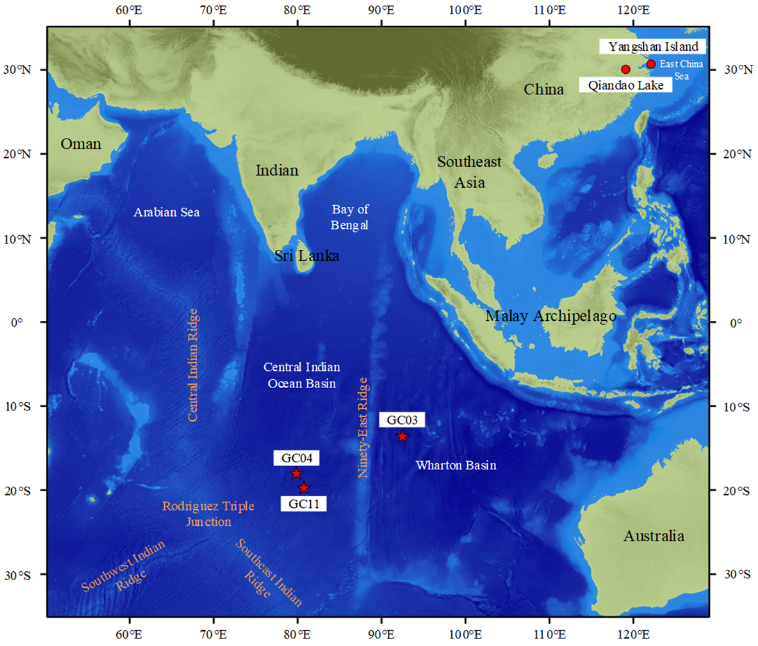

FIGURE 1
Sampling location map (the red stars represent the origin of the fossil fish teeth while the red circles represent the origin of the modern fish teeth). The base map was downloaded from GEBCO_2023 http://www.gebco.net and modified from Mukhopadhyay (1998).

approximately 60% of the total runoff (Li et al., 2011). Geologically, the Xin'an River Basin is located on the eastern margin of the Yangtze Plate, the upper reaches of the lake basin are the Neoproterozoic Jiangnan paleo island arc, and the lower reaches are the Early Paleozoic Huaiyushan-Tianmushan passive marginal basin (Pan et al., 2009). The carbonate rocks and clastic rocks of the early Paleozoic are exposed, and intrusive rocks and volcanic rocks of the Yanshan and Jinning periods have been developed (Tang et al., 2023).

2.3 Central Indian Ocean Basin

A series of NE-SW trending to NS-trending fault deformation belts divides the CIOB into the eastern and the western parts. The eastern CIOB is older (60-90 Ma), characterized by compressional structures, and presents a north-south trending fault zone, while the western is younger (30 Ma), including a NE-SW trending fault zone (Mukhopadhyay, 1998). Many of the isolated seamounts and seamount chains distributed parallel to the north-south trend in the basin are the products of a collision between the Indian plate and the Eurasian plate during the period of 65-49 Ma (Raju and Ramprasad, 1989; Dyment, 1993; Mukhopadhyay et al., 1997; Rajendran and Rao, 2000; Das et al., 2007). The Wharton Basin is located to the east of the CIOB, separated by the Ninety-East Ridge (NER). Based on the Fe-Mn crusts, the sources of detrital material change along the NER and reflect, from north to south, the decreasing influence of the Ganga River system and volcanic arcs located to the east, with the increasing influence of sediment derived from Australia to the south (Hein et al., 2016). The inhomogeneous growth of seamounts in the basin and the large amounts of volcanic-hydrothermal materials in volcanic rocks and sedimentary layers indicate the existence of volcanic hydrothermal activities in the plate (Iyer, 1991 and 2005; Mukhopadhyay, 1998; Iyer et al., 2007). Low-oxygen North Atlantic deep water (NADW) at 2,000–3,800 m and oxygen-rich Antarctic bottom water (AABW) below 3,800m converge to form circumpolar deep water. The redox condition at the sediment-water interface in the Indian Ocean is mainly regulated by export productivity and ventilation of abyssal water mass (Nambiar et al., 2022; Piotrowski et al., 2009).

3 Sampling and methods

3.1 Sampling

The modern fish teeth samples from the ECS include a *Miichthys miiuy*, a *Cynoglossus semilaevis*, a *Scomber japonicus*, and three *Larimichthys crocea* (numbered D_1, D_2, D_3, and D_4–D_6, respectively). Among them, *Miichthys miiuy* (D_1), *Scomber japonicus* (D_3), and *Larimichthys crocea* (D_4–D_6) are normal offshore bottom fishes. They live in a muddy and sandy environment and will migrate from deep water to the shore for long-distance reproductive migration during the reproductive season every year. By contrast, *Cynoglossus semilaevis* (D_2) are usually inert with slow action and only move in a small range. In addition, two *Mylopharyngodon piceus* (numbered QDH_1 and QDH_2) were collected from Qiandaohu Lake. They are bottom-living fish in fresh water, with reproductive migration generally from the lower reaches of rivers and their tributaries or affiliated lakes up to the middle and upper reaches.

Two sediment cores (GC04 and GC11) from the CIOB and one sediment core (GC03) from the Wharton Basin were collected using a gravity piston corer by the China Ocean Mineral Resources R & D Association (COMRA) during the 30th and 34th Dayang Cruises in 2014 and 2015.

GC04 was collected at 80.10° E, 17.54° S at a water depth of 4,826 m, 350 cm long, homogeneous, and was light reddish brown. In total, 14 subsamples were collected at intervals of 20–30 cm. GC11 was collected at 80.49° E, 19.54° S with a water depth of 5,106 m, 200 cm long, and was homogeneously reddish brown. In total, 21 subsamples were collected at 10 cm intervals. GC03 was collected at 92.41° E, 13.35° S with a water depth of 5072 m, 200 cm long, and was a heterogeneous texture with the upper part a yellowish-brown and the lower part a reddish-brown. In total, nine subsamples were collected at 10 cm intervals in the top 90 cm. The samples were cryopreserved at -20°C after collection and transported back to the laboratory for subsequent tests. In this study, 15 samples of debris of deposited fish teeth in three cores were identified and sorted under a binocular microscope.

3.2 Methods

An OLYMPUS CX43 microscope is used for transreflection photography of fish teeth at 5× magnification. After mounting in epoxy and polishing, samples were put into the TESCAN MIRA3 field emission microscope to take backscattered electron images (BSE).

3.2.1 Mineralogical analysis

Modern fish teeth D_5 and QDH_2 were selected as representatives for the laser Raman spectroscopy test (Horiba JY 800). The laser beam was directly aimed at the fish teeth for detection with an objective magnification of 50 and an excitation wavelength of 532 nm. The spectral acquisition beam range was 200–1,200 cm^{-1} with a slit of 100 μm, an aperture of 400 μm, and a grating of 1,800 gr/nm. The exposure time was 30 s and the data were interpreted using Origin 2018 software after the test.

3.2.2 Major element measurements

The major oxide compositions of the modern and fossil fish teeth were determined with an electron micro probe analysis (EMPA, JEOL JXA-iSP 100). The microprobe was operated at an accelerating voltage of 15.0 kV, a beam current of 10.0 nA, and a beam size of 5.0 μm. The experimental conditions for the surface analysis of D5 were accelerated at an accelerating voltage of 15.0 kV, a beam current of 20.0 nA, and a minimum beam size. Data were corrected online using a modified ZAF [atomic number (Z) effect, absorption (A) effect, and fluorescence excitation (F) effect] correction procedure.

3.2.3 Trace element measurements

A laser ablation inductively coupled plasma mass spectrometer (LA-ICP-MS) was used to analyze trace elements in fossil and modern fish teeth. The Resolution SE 193 nm excimer laser was coupled to an Agilent Model 7900 inductively coupled plasma mass spectrometer. Samples analysis was conducted at or near the EMPA spot locations under laser conditions with a beam spot diameter of 38 μm, denudation frequency of 10 Hz, and energy density of 4 J/cm^2. The trace element concentrations of the fish teeth were calibrated against the standard reference materials (National Institute of Standards and Technology (NIST) 610 and NIST 612). Suitable internal standards (BHVO-2G and BIR-1G from the United States Geological Survey) were also carried out for the data calibration. During the test, two NIST 610 standard samples and one of each NIST612, BHVO-2G, and BIR-1G standard samples were analyzed every eight sample points. The relative standard deviations of most of the trace elements of the standards were within 5%. The concentration of trace elements was calculated using the Calcium (Ca) element as the internal standard based on the electron probe data at each measuring point. Specifically, we performed an *in-situ* LA-ICP-MS test at the same point as the electron probe test. This test and data correction method can ensure the consistency and reliability of trace element data, and avoid the systematic error caused by a fixed internal standard. The software Iolite V4.0 was adopted for data processing (Paton et al., 2011).

3.2.4 $^{87}Sr/^{86}Sr$-$^{143}Nd/^{144}Nd$ isotopic ratios

$^{87}Sr/^{86}Sr$ and $^{143}Nd/^{144}Nd$ isotopic ratios were analyzed *in situ* in low resolution and static mode using a Neptune Plus Multi-Collector Inductively Coupled Plasma Mass Spectrometer (MC-ICP-MS) (Thermo Fisher Scientific, Germany) coupled to a J-200 343 nm femto second laser ablation system (Applied Spectra, USA).

At the beginning of every analytical session, the fs-LA-ICP-MS system was optimized using NIST 612 to achieve the maximum signal intensity and low oxide rates. The samples were ablated in line mode with a spot size of 30 μm, a line length of 20 μm, a stage movement speed of 0.65 μm/s, a laser repetition rate of 8 Hz, and a beam energy density of 1.5 J/cm^2.

The instrumental mass bias for the Sr isotopes was corrected using an exponential function based on the $^{86}Sr/^{88}Sr$ value of 0.1194. Correction of the interferences of the Krypton (^{84}Kr) and ^{86}Kr isotopes was successfully accomplished by background subtraction. The interferences of the doubly charged ions of Erbium ($^{168}Er^{2+}$) on ^{84}Sr, $^{170}Er^{2+}$ and Ytterbium ($^{170}Yb^{2+}$) on Rubidium (^{85}Rb), $^{172}Yb^{2+}$ on ^{86}Sr, and $^{174}Yb^{2+}$ on ^{87}Sr were corrected based on the measured signal intensities of $^{167}Er^{2+}$ (m/z 83.5) and $^{173}Yb^{2+}$ (m/z 86.5) and the natural isotopic compositions of Rb, Er, and Yb (Li et al., 2018). As for the Nd and Samarium (Sm) isotopes, the instrumental mass biases were corrected by an exponential function based on the $^{146}Nd/^{144}Nd$ value of 0.7219 and the $^{147}Sm/^{149}Sm$ value of 1.0868, respectively (Yang et al., 2014). The interference of ^{143}Sm on ^{143}Nd was corrected for the mass bias coefficient and the natural isotopic composition based on the measured signal intensity of ^{147}Sm. To monitor the instrument's stability and for external correction of the $^{147}Sm/^{144}Nd$ ratios, the Durango and MAD apatite reference standards were analyzed. The relative standard deviations of the Sr and Nd isotopes of standards were within 2%.

Due to the contents of Nd in marine and lake fish teeth being below the limit of detection, the Nd isotopes in modern fish teeth were not obtained. The Nd isotopic compositions are generally expressed as εNd (t=0) ($\varepsilon Nd = [\frac{^{143}Nd/^{144}Nd_{Sample}}{^{143}Nd/^{144}Nd_{CHUR}} - 1] \times 10^4$), where $(^{143}Nd/^{144}Nd)_{Sample}$ is the value of the actual sample and $(^{143}Nd/^{144}Nd)_{CHUR}$ is the value of the chondritic uniform reservoir, calculated using $(^{143}Nd/^{144}Nd)_{CHUR}=0.512630$ (Bouvier et al., 2008).

4 Results

4.1 Morphology and mineralogical characteristics

Fossil and modern fish teeth show distinct morphological characteristics respectively. The teeth of the *Mylopharyngodon piceus* from Qiandaohu Lake are approximately 5 mm in width and length showing a nightcap style (Figure 2b). In contrast, the teeth of marine fish from the ECS are tapered, and smaller with a length of approximately 1 mm (Figure 2a). The fossil fish teeth show similar morphology and structure to the modern marine fish teeth but were much smaller with only 100–250 μm and/or less. Beside cones, the fossil fish teeth also showed ellipses, spindles, long stripes, and other shapes (Figure 2c). All fish teeth have a two-layer structure of enamel and dentin. The dentin is inside the fish teeth with obvious pores, indicating a relatively loose texture. The enamel is a thin light-colored dense outer layer of the fish teeth (Figure 2), which exhibits the typical growth structure clearly.

The marine fish teeth and lake fish teeth in this study had similar Raman spectra with four vibration modes of apatite $[PO_4]^{3-}$, indicating that the main component is hydroxyphosphate. The enamel showed a generally higher peak intensity than that of dentin (Figure 3). The main peak of marine fish teeth enamel was 1,030 cm^{-1} (Figures 3a, b), representing the A-type substitution of carbonate (that is, the substitution of hydroxyl), while the main peak of lake fish teeth enamel was 1070 cm^{-1} (Figures 3e, f), representing the B-type substitution of carbonate (that is, the substitution of phosphate). There were both A-type and B-type substitutions in the dentin of the marine and lake fish teeth.

A similar double-layer structure in fossil fish teeth was indicated, and both the enamel and dentin of fossil fish teeth are composed of hydroxyapatite. Moreover, the x-ray diffraction (XRD) of the enamel also showed a higher peak than that of dentin, indicating higher crystallinity of enamel (Liao et al., 2019a).

Elements mapping of the living fish teeth (sample D_5 as an example) showed that the major elements vary in the profile (Figure 4). The contents of fluorine (F), natrium (Na), phosphorus (P), calcium (Ca), and ferrum (Fe) increased from the root to the tip and decreased from the enamel to the central dentin. In contrast, the contents of magnesium (Mg) increased from the root to the tip, and from the lateral enamel to the medial dentin. Sr and sulfur (S) were evenly distributed in the dentin and enamel of fish teeth without an obvious tendency.

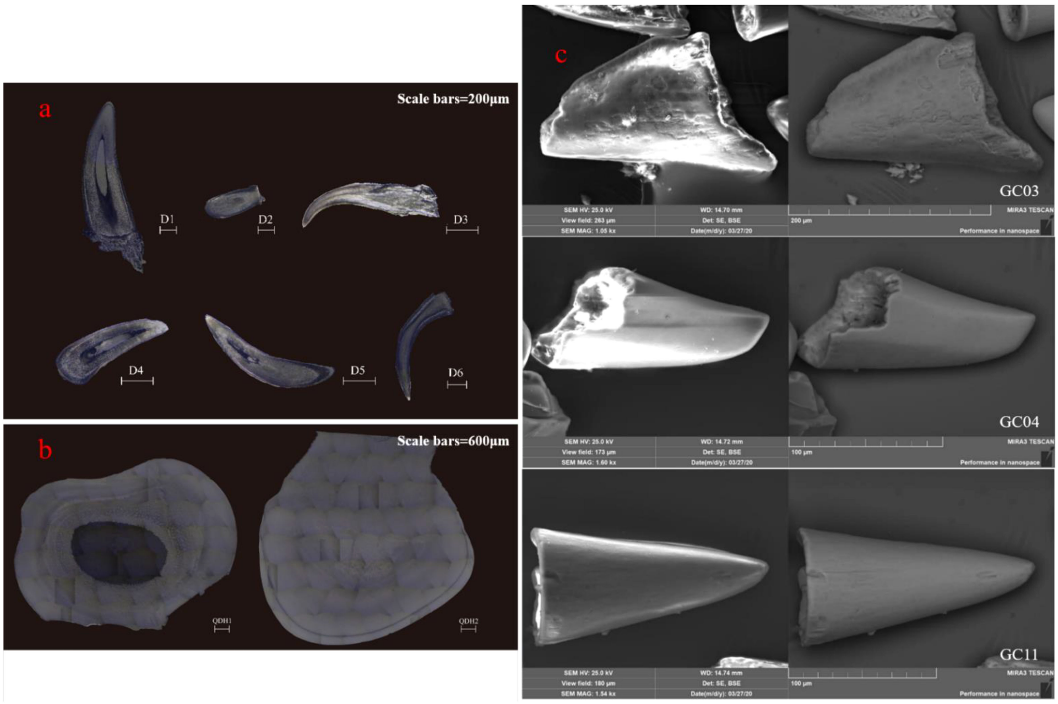

FIGURE 2
Comparison of the morphological features of fish teeth based on BSE photos: **(a)** Modern fish teeth from the ECS; **(b)** Modern fish teeth from Qiandaohu Lake; **(c)** Representative fossil fish teeth from the CIOB.

4.2 Major element composition

The main element compositions of both fossil and modern fish teeth are CaO and P_2O_5, and there is a significant positive correlation between them (Figure 5a). Generally, the fossil fish teeth are characterized by higher contents but narrower fluctuations of CaO (44.32%–51.96%) and P_2O_5 (36.03%–40.73%) than the modern fish teeth (29.00%–48.49% for CaO and 24.77%–42.36% for P_2O_5) as shown in Table 1. CaO/P_2O_5 in the fish teeth was broader than the stoichiometric ratio of apatite (10/6) but was basically within the range of CaO/P_2O_5 in fossil fish teeth and mammal bones samples studied previously [from 1.2 to 2.0, Nemliher et al. (2004)]. CaO/P_2O_5 in the fossil fish teeth varied in the range of 1.19 to 1.39, while CaO/P_2O_5 in the modern fish teeth varied in the range of 1.00 to 1.27. The higher CaO/P_2O_5 in the fossil fish teeth may indicate the influence of the fossilization and diagenesis with the replacement of orthophosphate-ion by carbonate-ion in the apatite crystal lattice (Nemliher et al., 2004).

Except for CaO and P_2O_5, F had the highest content in the fossil fish teeth, ranging from 0.94% to 3.12%. It was much higher than the modern fish teeth with 0.00%–1.05%. Furthermore, the fossil fish teeth were also distinctly more enriched in Na_2O, FeO, and SiO_2 (Table 1), which may be due to the porous particles with inclusions of terrigenous material after deposition (Nemliher et al., 2004). The lowest CaO/P_2O_5 was observed in GC03 (as shown in Table 1), together with significantly higher contents of Al_2O_3, SiO_2, and K_2O than GC04 and GC11, suggesting intense influence from terrigenous materials in core GC03 as well. Inversely, the modern fish teeth had higher MgO, K_2O, and chlorine (Cl) (Table 1). As essential mineral elements for fish life, teeth, bone, and scales are important sinks of these elements (Bijveld s et al., 1998).

4.3 Trace element composition

Generally, most trace elements were detected in fossil fish teeth and varied greatly. Some trace elements including beryllium (Be), germanium (Ge), cadmium (Cd), indium (In), thallium (Tl), bismuth (Bi), and most REEs (except lanthanum, cerium, yttrium) were below the limit of detection in both the marine and lake fish teeth. Vanadium (V), nickel (Ni), arsenic (As), stannum (Sn), and thorium (Th) only in the marine fish teeth while Hf was detected only in the lake fish teeth (Table 2).

4.3.1 Trace elements in modern fish teeth

The marine and lake fish teeth had different contents of trace elements. Using the ratio of element contents of marine fish teeth to those in lake fish teeth (M_i/L_i = element i in marine fish teeth/in lake fish teeth) as shown in Figure 6, the trace elements can be divided into three categories:

1. Strontium (Sr), copper (Cu), scandium (Sc), cobalt (Co), uranium (U), titanium (Ti), ferrum (Fe), niobium (Nb), lead (Pb), barium (Ba), gallium (Ga), manganese (Mn), chromium (Cr), lithium (Li), cesium (Cs), nickel (Ni), vanadium (V), and arsenic (As) had higher contents in marine fish teeth than in lake fish teeth. Among them, Mn

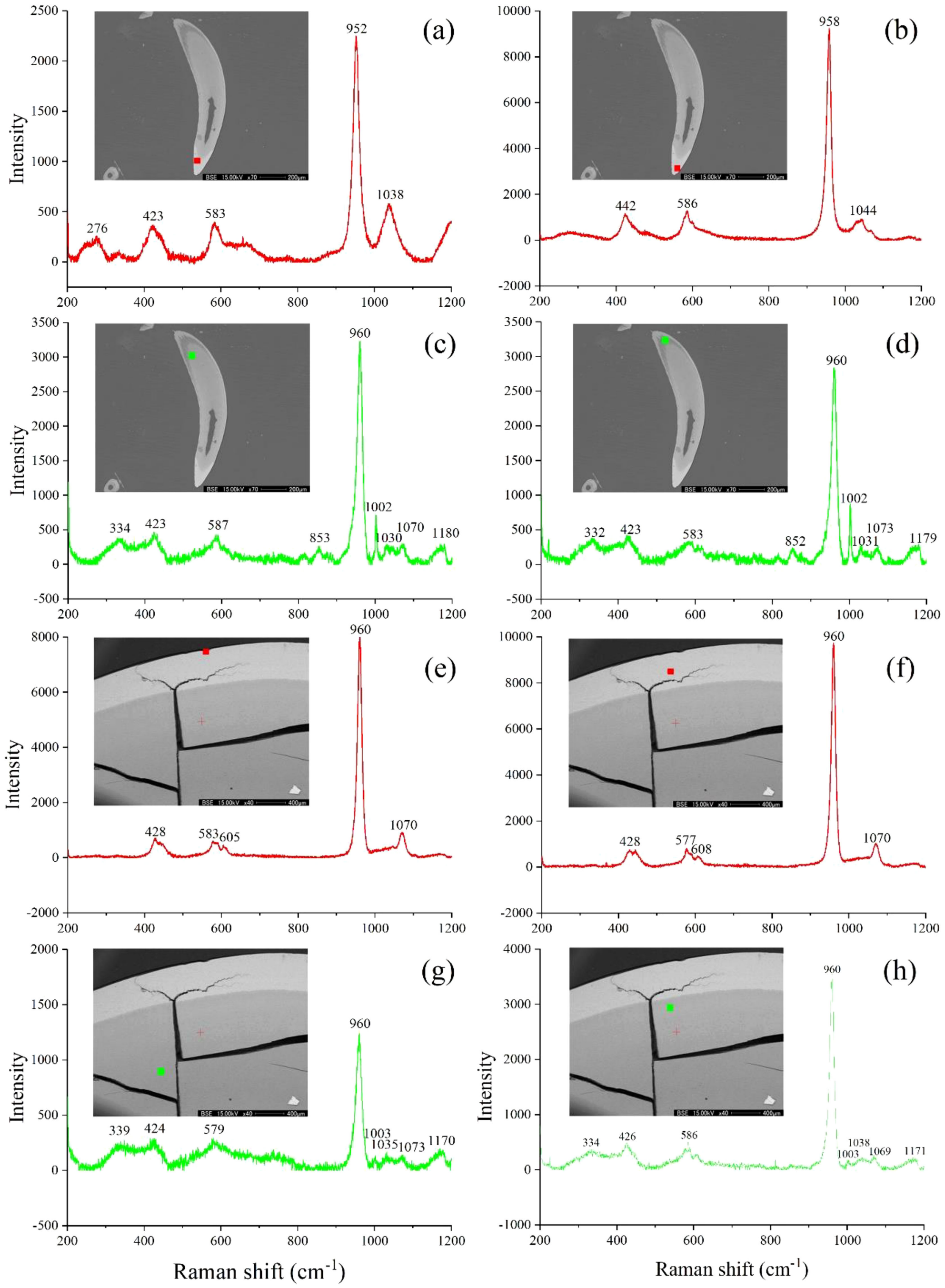

FIGURE 3
Raman spectra of modern fish teeth [**(a–d)**: marine fish teeth D_5, where **(a, b)** are in the enamel; **(c, d)** are in the dentin; **(e–h)**: lake fish teeth QDH_2, where **(e, f)** are in the enamel, **(g, h)** are in the dentin].

and U had M_i/L_i ratios higher than 5, reflecting the obvious enrichment in marine fish teeth. Nb, Pb, Li, and Sr were moderately enriched with M_i/L_i ratios of 2–5. Cu, Sc, Co, Ti, Fe, Ba, Ga, and Cr were slightly enriched in marine fish teeth with M_i/L_i ratios of 1–2.

2. Zirconium (Zr), molybdenum (Mo), tungsten (W), zinc (Zn), and rubidium (Rb), with M_i/L_i ratios of <1, were deficient in marine fish teeth and could be sorted as W (0.07) < Mo (0.17) < Rb (0.51) < Zn (0.55) < Zr (0.90).
3. The M_i/L_i ratios of Beryllium (Be), germanium (Ge), stannum (Sn), cadmium (Cd), indium (In), hafnium (Hf), thallium (Tl), thorium (Th), bismuth (Bi), and rare earth elements (REEs), were unavailable due to their absence in marine fish teeth and/or lake fish teeth.

To analyze the ability of fish to aggregate trace elements over the life cycle, the enrichment index of trace elements of modern marine fish teeth was calculated relative to the seawater around Yangshan

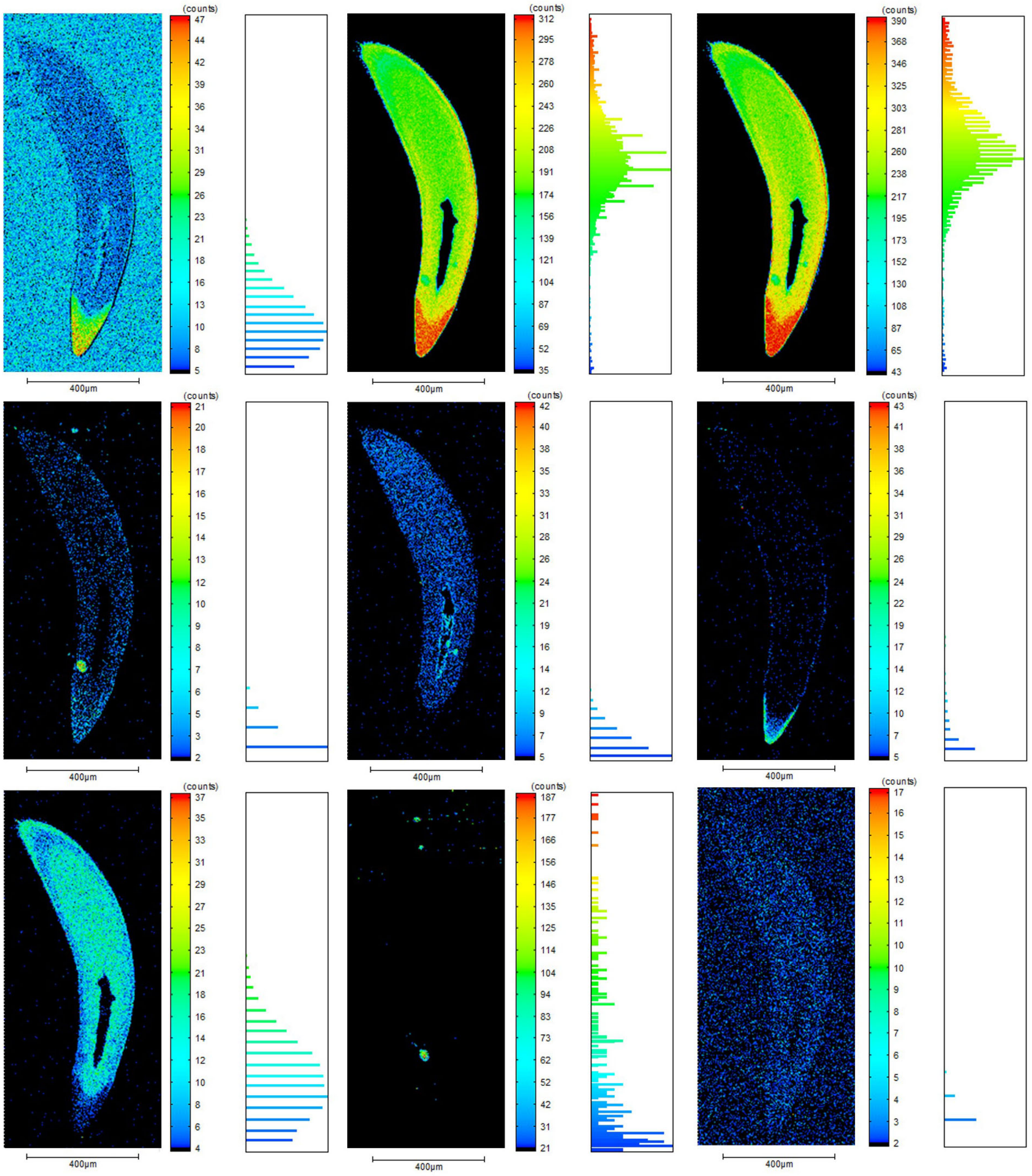

FIGURE 4
Profile distribution characteristics of major elements in typical marine fish teeth (D_5).

Island (Zeng et al., 2012) (M_i/W_i = element i in marine fish teeth/seawater). The lake fish teeth were not considered due to a lack of reliable background values of trace element content in the water bodies of the Xin'an River Basin. The elements that were absent in marine fish teeth were also not included. It was indicated that the M_i/W_i ratio for marine fish teeth varied greatly in the range from lower than 10^{-1} to higher than 10^3, as shown in Table 3 and Figure 6. Most of them were higher than 1, indicating obvious enrichment. Rb was the only deficit trace element with a M_i/W_i of 0.39. Cu, Co, Pb, Ba, W, Zn, Cr, and Sr were highly enriched with a M_i/W_i higher than 10^2, and Mn, Ga, Zr, Sn, and Th had a M_i/W_i higher than 10^3.

4.3.2 Trace elements in fossil fish teeth

The trace element composition of fossil fish teeth in core sediments of the Indian Ocean was compared with that of modern marine fish teeth (F_i/M_i = element i in fossil fish teeth/marine fish teeth). To analyze the trace elements enrichment degree of fish teeth after deposition, grading with a 10-fold gradient was used, as shown in Figure 6.

Type I: slightly enriched with F_i/M_i of 1–10, including Sr, Li, Sn, Rb, Zn, Cr, Mn, Ga, As, and Ba. Among them, Sr had the lowest ratio of 1.13.

Type II: moderately enriched with F_i/M_i between 10–100, including W, Pb, V, Ni, Nb, Fe, Ti, Cs, and Mo.

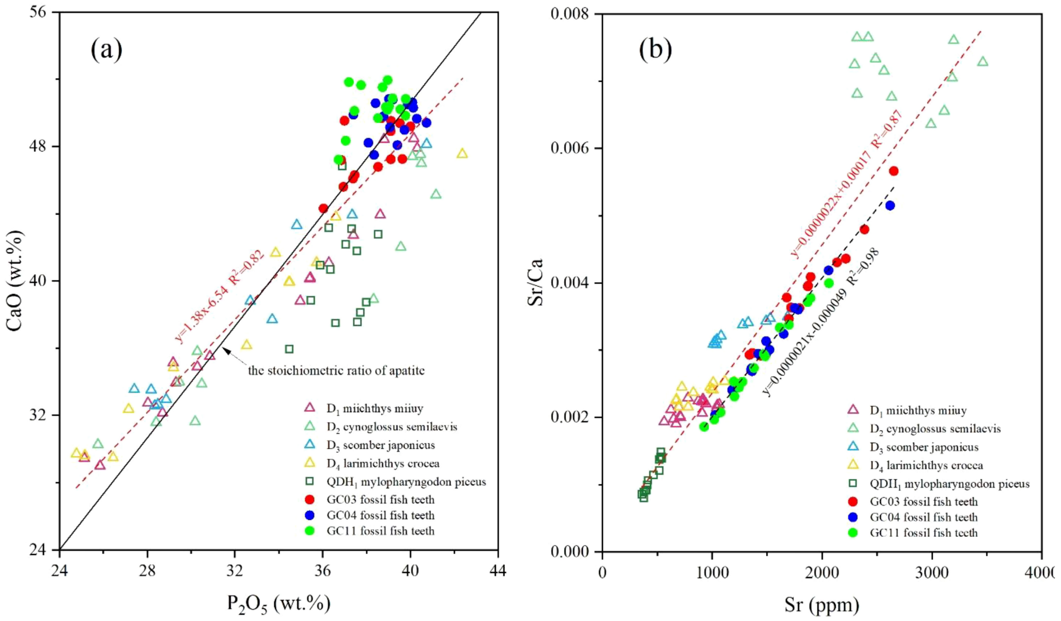

FIGURE 5
(a) CaO/P_2O_5 and **(b)** Sr/Ca ratios of fish teeth in this study. CaO and P_2O_5 data are from major element concentrations tested by EMPA and summarized in Table 1, while Sr data are from trace element concentrations tested by LA-ICP-MS and summarized in Table 2.

Type III: highly enriched with F_i/M_i between 100–1,000, including U, Co, Sc, and Cu.

Type IV: extremely enriched with F_i/M_i higher than 1,000, with only two elements, Zr and Th, belonging to this type.

Besides the above four categories, there were special types of trace elements that were absent in modern marine fish teeth but present in fossil fish teeth. Among them, REEs were extremely high in fossil fish teeth, reaching 7,546.72 ppm (Table 4). Be and Ge had high concentrations in fossil fish teeth as well, with 4.03 ppm and 25.87 ppm (Table 2), respectively. In addition, the concentrations of Cd (0.65 ppm), In (0.03 ppm), Hf (0.5 ppm), Tl (0.11 ppm), and Bi (0.07 ppm) were observed to be low in the fossil fish teeth. It was deduced that these elements were aggregated in the fossil fish teeth after deposition.

In summary, trace elements with enhanced concentrations after deposition include the rare and rare earth elements family, represented by Zr, Th, Sc, and REEs with significant enrichment, followed by iron family elements, such as Ti, V, Fe, Co, Ni and Cu, with no obvious enrichment of rock-forming family elements such as Ba, Rb, Li, and Sr, in fossil fish teeth. It is noteworthy that REEs were highly enriched after deposition, which was obviously different from the enrichment of Sr during the life cycle of fish. The distinctly different enrichment procedures of REEs and Sr are an important basis for source tracing when using their respective isotopes.

Furthermore, compared with GC04 and GC11, the fossil fish teeth from GC03 contained higher concentrations of Sc, V, Zn, Sr, Zr, Mo, Hf, W, and U but significantly lower concentrations of Fe, Ni, Ga, Rb, Sn, and Cs (Table 2).

M_i/W_i represents the ratio of marine fish teeth/Yangshan sea water (data from Zeng et al. (2012)); F_i/M_i represents the ratio of fossil fish teeth/marine fish teeth; Mi/Li represents the ratio of marine fish teeth/lake fish teeth.

(Due to their non-detection in fish teeth, the concentration coefficients of Be, Ge, Cd, In, Hf, Tl, Bi, Th, Ti, Nd, and REE could not be calculated.

4.3.3 Rare earth elements in fossil fish teeth

The REE in the fossil fish teeth is further discussed in detail. Table 4 shows the REE content in fossil fish teeth from the three cores. The concentrations of ΣREEs in the fossil fish teeth varied greatly from hundreds to thousands of ppm. The average values of REEs can be sorted as GC03 (8,971.93 ppm) > GC11 (7,690.59 ppm) > GC04 (5,707.63 ppm).

The highest REE concentration in GC03 was aligned with higher concentrations of Sc, V, Zn, Sr, Zr, Hf, Mo, W, and U (Table 2). The symbiosis of these elements in fossil fish teeth is obviously closely related to the isomorphism of these elements to Ca^{2+} in fish tooth apatite. Generally, U in the apatite is positively related to P by absorbance, co-deposits, or substitution with Ca (Hughes and Rakovan, 2002; Pan and Fleet, 2002). Therefore, U together with REEs, can be accumulated by fish teeth in deep-sea sediments (Li et al., 2023). The relatively low Ca/P ratio of the fossil fish teeth from the GC03 may be important in explaining the enriched REEs and U, which is consistent with the distinct negative correlation between REEs and CaO/P_2O_5 in REE-rich sediments (Zhang et al., 2017).

Similar to previous studies, distinct fractionation of REEs was observed in the fossil fish teeth. The normalized REE patterns of the post-Archean mean shales of Australia [PAAS, Taylor and McLennan (1985)] (as shown in Figure 7) have been shown to be consistent with fossil fish teeth in the Pacific Ocean and the Indian Ocean in previous studies (Liao et al., 2019a; Sun et al., 2022; Liao

TABLE 1 The content of major elements in fossil fish teeth and modern fish teeth.

wt.%		CaO	P_2O_5	Na_2O	Al_2O_3	MgO	SO_3	SrO	FeO	K_2O	SiO_2	F	Cl	CaO/ P_2O_5
GC03 fish teeth	Min	44.32	36.03	0.93	0.04	0.13	0.12	0.02	0.04	0.01	0.03	0.94	0.00	1.19
	Max	50.78	39.99	1.68	0.51	0.61	1.35	0.26	0.16	0.13	3.14	3.12	0.07	1.34
	Ave	47.86	38.34	1.30	0.14	0.31	0.69	0.15	0.10	0.04	0.72	2.14	0.03	1.25
	SD (n=15)	1.85	1.28	0.20	0.14	0.15	0.29	0.06	0.04	0.04	1.11	0.51	0.02	0.04
GC04 fish teeth	Min	47.51	37.39	1.03	0.01	0.11	0.16	0.13	0.08	0.01	0.03	1.07	0.01	1.21
	Max	50.84	40.73	1.40	0.01	0.35	1.11	0.32	0.51	0.02	0.34	2.84	0.09	1.33
	Ave	49.63	39.23	1.25	0.01	0.20	0.47	0.20	0.19	0.01	0.10	2.07	0.04	1.27
	SD (n=15)	1.06	0.93	0.10	/	0.07	0.22	0.07	0.15	0.01	0.10	0.41	0.02	0.04
GC11 fish teeth	Min	47.22	36.71	0.72	0.04	0.06	0.12	0.05	0.01	0.01	0.03	1.07	0.02	1.25
	Max	51.96	39.78	1.34	0.06	0.28	0.66	0.25	0.45	0.01	0.19	2.66	0.09	1.39
	Ave	50.34	38.50	1.13	0.05	0.14	0.39	0.13	0.13	0.01	0.08	2.18	0.04	1.31
	SD (n=15)	1.28	1.01	0.15	0.01	0.06	0.16	0.05	0.14	0.00	0.05	0.43	0.02	0.04
The sum of fossil fish teeth	Min	44.32	36.03	0.72	0.01	0.06	0.12	0.02	0.01	0.01	0.03	0.94	0.00	1.19
	Max	51.96	40.73	1.68	0.51	0.61	1.35	0.32	0.51	0.13	3.14	3.12	0.09	1.39
	Ave	49.28	38.69	1.23	0.11	0.22	0.52	0.16	0.13	0.03	0.30	2.13	0.04	1.27
	SD (n=45)	1.76	1.13	0.17	0.13	0.12	0.26	0.06	0.11	0.03	0.68	0.44	0.02	0.04
Marine fish teeth	Min	29.00	24.77	0.26	0.00	0.19	0.06	0.02	0.01	0.01	0.00	0.00	0.03	1.02
	Max	48.49	42.36	1.32	0.33	2.43	0.67	0.57	0.42	0.21	0.08	1.05	0.17	1.27
	Ave	38.49	33.16	0.57	0.09	0.74	0.45	0.19	0.06	0.08	0.03	0.15	0.08	1.16
	SD (n=54)	6.14	5.10	0.24	0.09	0.42	0.17	0.12	0.09	0.05	0.02	0.21	0.04	0.05
Lake fish teeth	Min	35.95	34.47	0.27	0.00	0.70	0.05	0.01	0.01	0.01	0.02	0.00	0.06	1.00
	Max	46.85	38.51	0.97	0.04	3.18	0.44	0.10	0.06	0.08	0.10	0.10	0.18	1.27
	Ave	40.60	36.83	0.47	0.02	1.85	0.20	0.06	0.03	0.05	0.04	0.05	0.09	1.10
	SD (n=14)	2.96	1.08	0.18	0.01	0.84	0.10	0.03	0.02	0.02	0.02	0.03	0.03	0.08

et al., 2022; Deng et al., 2022) with $(La/Yb)_N < (La/Sm)_N < (Sm/Yb)_N$. The REE distribution pattern was consistent with the bottom seawater of the Indian Ocean [data from Nozaki and Alibo (2003)], with strong negative Ce anomalies (range from 0.01 to 0.26) and slight positive Y anomalies (ranging from 1.04 to 1.46).

It is noteworthy that the REE normalization pattern between fossil fish teeth was significantly different from that of deep-sea sediments in this study (Figure 7). The sediments of GC04 and GC11 in the CIOB showed a slight left-leaning flat type, and the sediments of GC03 from the Wharton Basin showed a right-leaning flat type. But all the fossil fish teeth showed an obvious strong negative Ce anomaly and a weak positive Y anomaly. The distinct differences in REE normalization patterns between the sediments and fossil fish teeth in this study were different from those from the Pacific Ocean where the REE normalization patterns in the sediments and fossil fish teeth were consistent and showed an obvious negative Ce anomaly and a positive Y anomaly (Bi et al., 2021; Ren et al., 2022; Sa et al., 2018; Liao et al., 2019a).

The bulk sediments data of GC03, GC04, and GC11 are from Zhang et al. (2023); the bulk sediments data of the Pacific Ocean are from Sa et al. (2018); the Indian Ocean fish teeth data are from Sun et al. (2022); the North Pacific fish teeth data are from Liao et al. (2019a); the Western Pacific fish teeth data are from Deng et al. (2022); the Southeast Pacific fish teeth data are from Liao et al. (2022); the Indian ocean deep water data are from Nozaki and Alibo (2003).

4.4 $^{87}Sr/^{86}Sr$-$^{143}Nd/^{144}Nd$ isotope ratios

Due to the extremely low Nd content in the modern fish teeth, the $^{143}Nd/^{144}Nd$ ratio was available only in the fossil fish teeth. The $^{87}Sr/^{86}Sr$ values of the modern fish teeth are shown in Table 5 and 6 exhibits the $^{143}Nd/^{144}Nd$ ratio and $^{87}Sr/^{86}Sr$ values for the fossil fish teeth.

The $^{87}Sr/^{86}Sr$ of marine fish teeth was less radiogenic but fluctuated in a wider range (from 0.70633 to 0.70913, with an average of 0.70832) than that of the lake fish teeth (from 0.70918 to 0.70973, with an

TABLE 2 The content of trace elements in fossil fish teeth and modern fish teeth.

ppm		Li	Be	Sc	Ti	V	Cr	Mn	Fe	Co	Ni	Cu	Zn	Ga	Ge	As	Rb
GC03 fish teeth	Min	1.82	0.97	4.30	1.38	2.21	4.37	35.90	202.10	0.02	2.28	11.36	38.06	0.62	8.10	0.68	0.08
	Max	6.36	8.13	315.00	261.30	37.25	15.00	1290.00	2374.00	5.77	61.20	598.00	777.00	21.82	80.00	26.61	1.41
	Ave	3.66	4.71	151.08	105.17	19.23	6.86	440.09	789.47	1.53	16.96	181.65	315.48	7.97	31.68	10.91	0.67
	SD (n=15)	1.36	2.31	77.38	67.17	11.48	4.06	386.15	532.28	1.89	15.42	169.13	209.32	6.14	19.74	6.63	0.35
GC04 fish teeth	Min	2.14	1.54	16.50	7.00	3.12	4.17	8.21	75.00	0.01	0.31	37.20	97.50	1.65	1.74	1.64	0.04
	Max	22.60	9.15	232.00	540.00	31.40	23.30	389.00	12500.00	5.60	112.00	511.00	568.20	59.00	54.80	19.10	30.50
	Ave	4.91	5.19	98.91	77.91	10.38	8.53	128.37	1259.75	0.59	25.57	191.02	275.95	9.67	18.97	7.00	2.36
	SD (n=15)	5.01	2.34	79.84	130.37	6.81	7.29	125.90	3125.40	1.40	38.58	159.79	140.07	14.20	15.21	4.87	7.79
GC11 fish teeth	Min	1.94	0.13	4.34	1.71	2.13	7.40	21.70	126.30	0.06	0.70	17.83	87.90	0.85	2.37	0.99	0.08
	Max	51.00	7.86	227.90	970.00	37.10	295.00	7800.00	14700.00	207.00	259.00	355.60	823.00	47.00	69.60	28.90	17.80
	Ave	11.77	2.17	77.76	106.29	9.34	63.39	705.55	2213.71	24.13	29.38	104.48	276.45	8.63	27.33	10.12	2.01
	SD (n=15)	13.82	1.79	61.39	251.87	10.66	99.74	2048.71	3832.16	60.54	70.09	98.56	175.92	13.95	22.27	8.29	4.48
The sum of fossil fish teeth	Min	1.82	0.13	4.30	1.38	2.13	4.17	8.21	75.00	0.01	0.31	11.36	38.06	0.62	1.74	0.68	0.04
	Max	51.00	9.15	315.00	970.00	37.25	295.00	7800.00	14700.00	207.00	259.00	598.00	823.00	59.00	80.00	28.90	30.50
	Ave	6.78	4.03	109.25	96.23	12.98	29.97	417.78	1402.96	8.03	23.97	159.05	289.29	8.76	25.87	9.34	1.68
	SD (n=45)	9.07	2.50	78.13	162.36	10.63	66.84	1186.70	2839.86	34.12	46.18	147.83	174.31	11.77	19.57	6.80	5.13
Marine fish teeth	Min	0.87	/	0.43	0.65	0.48	4.45	12.57	15.03	0.11	0.41	0.27	18.28	0.32	/	0.72	0.11
	Max	11.25	/	0.61	3.87	0.82	20.23	188.55	362.66	0.15	3.90	7.57	152.38	4.20	/	1.75	1.02
	Ave	3.16	/	0.52	2.26	0.71	6.70	59.86	43.58	0.13	1.20	0.74	70.40	1.22	/	1.22	0.41
	SD (n=54)	2.14	/	0.13	2.28	0.13	3.53	37.88	65.86	0.03	1.12	1.04	34.10	0.76	/	0.37	0.20
Lake fish teeth	Min	1.15	/	0.38	1.40	/	5.13	7.11	20.98	0.104	/	0.26	66.45	0.46	/	/	0.35
	Max	1.51	/	0.40	1.40	/	6.96	10.29	97.53	0.104	/	1.23	187.14	0.96	/	/	1.39
	Ave	1.29	/	0.39	1.40	/	5.96	8.75	30.80	0.104	/	0.56	128.30	0.64	/	/	0.80
	SD (n=14)	0.19	/	0.01	/	/	0.85	1.30	19.86	/	/	0.25	41.03	0.15	/	/	0.38
ppm		Sr	Zr	Nb	Mo	Cd	In	Sn	Cs	Ba	Hf	W	Tl	Pb	Bi	Th	U
GC03 fish teeth	Min	1338.00	1.23	0.14	0.74	0.26	0.021	0.22	0.009	6.27	0.14	0.16	0.03	0.28	0.03	0.13	0.83
	Max	2652.00	275.00	0.52	10.72	1.31	0.072	1.33	0.023	233.60	1.38	0.93	0.40	23.60	0.09	81.70	32.05
	Ave	1832.67	120.50	0.29	4.76	0.56	0.039	0.49	0.016	84.60	0.59	0.53	0.11	5.50	0.05	22.99	21.30

(Continued)

TABLE 2 Continued

ppm		Sr	Zr	Nb	Mo	Cd	In	Sn	Cs	Ba	Hf	W	Tl	Pb	Bi	Th	U
	SD (n=15)	382.33	66.91	0.12	2.79	0.26	0.016	0.33	0.011	65.04	0.33	0.26	0.11	5.60	0.02	24.48	7.87
GC04 fish teeth	Min	1024.00	12.10	0.10	0.17	0.26	0.005	0.18	0.023	16.18	0.10	0.01	0.02	1.50	0.01	0.11	3.07
	Max	2618.00	216.00	1.35	3.96	1.31	0.099	2.02	2.900	610.00	2.80	0.97	0.35	18.00	0.20	52.10	27.69
	Ave	1551.33	74.26	0.53	1.04	0.74	0.030	0.62	0.984	99.66	0.45	0.30	0.06	5.39	0.05	12.04	17.74
	SD (n=15)	393.20	61.12	0.71	1.01	0.35	0.027	0.60	1.659	146.94	0.75	0.39	0.08	4.84	0.05	14.62	7.96
GC11 fish teeth	Min	926.30	1.47	0.10	0.14	0.32	0.007	0.29	0.069	8.20	0.14	0.10	0.02	1.92	0.03	1.43	0.39
	Max	2061.00	149.50	3.80	16.70	0.80	0.066	4.10	1.030	467.00	0.99	1.95	0.77	56.80	0.89	316.00	24.66
	Ave	1426.35	49.19	0.81	3.67	0.58	0.030	1.29	0.307	84.45	0.40	0.68	0.16	8.59	0.12	57.36	9.53
	SD (n=15)	341.25	45.30	1.47	4.73	0.19	0.024	1.31	0.410	135.12	0.30	0.67	0.21	13.49	0.24	87.85	6.57
The sum of fossil fish teeth	Min	926.30	1.23	0.10	0.14	0.26	0.005	0.18	0.009	6.27	0.10	0.01	0.02	0.28	0.01	0.11	0.39
	Max	2652.00	275.00	3.80	16.70	1.31	0.099	4.10	2.900	610.00	2.80	1.95	0.77	56.80	0.89	316.00	32.05
	Ave	1603.45	81.32	0.50	3.12	0.65	0.034	0.76	0.452	89.57	0.50	0.51	0.11	6.50	0.07	30.80	16.19
	SD (n=45)	402.85	64.48	0.87	3.53	0.30	0.022	0.83	0.914	118.65	0.50	0.43	0.14	8.81	0.14	55.64	8.86
Marine fish teeth	Min	561.97	0.02	0.015	0.02	/	/	0.24	0.006	2.35	/	0.01	/	0.03	/	0.003	0.00
	Max	3462.87	0.09	0.023	0.10	/	/	0.24	0.007	39.71	/	0.21	/	1.23	/	0.003	0.43
	Ave	1425.18	0.06	0.019	0.06	/	/	0.24	0.007	9.88	/	0.04	/	0.36	/	0.003	0.09
	SD (n=54)	827.54	0.03	0.006	0.03	/	/	/	0.001	7.08	/	0.05	/	0.32	/	/	0.12
Lake fish teeth	Min	358.87	0.01	0.0056	0.07	/	/	/	/	4.32	0.007	0.19	/	0.03	/	/	0.002
	Max	540.40	0.14	0.0061	2.14	/	/	/	/	9.16	0.007	1.19	/	0.52	/	/	0.011
	Ave	455.10	0.07	0.0059	0.33	/	/	/	/	5.75	0.007	0.58	/	0.16	/	/	0.005
	SD (n=14)	71.62	0.05	0.0003	0.54	/	/	/	/	1.42	/	0.34	/	0.13	/	/	0.003

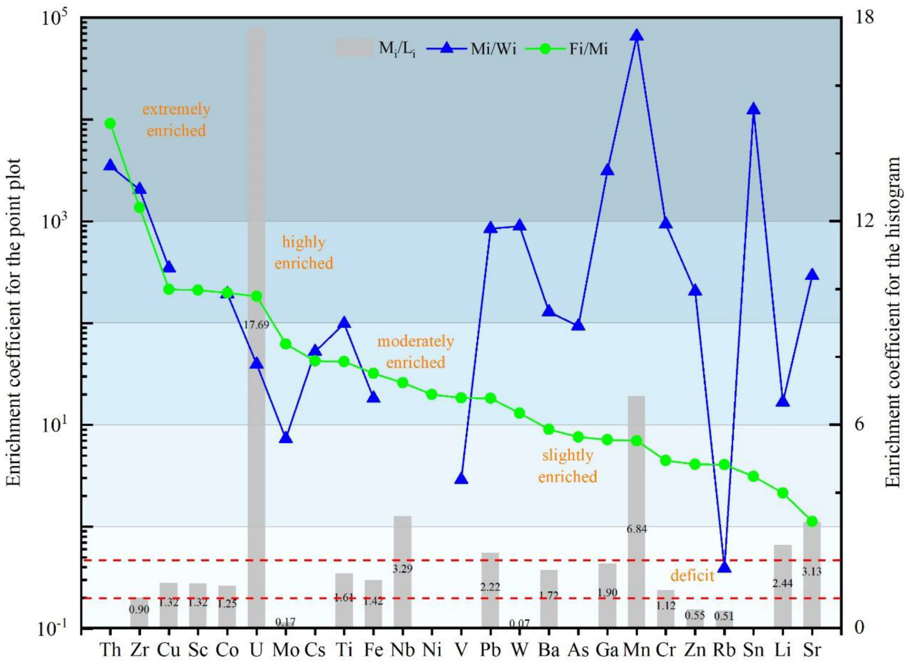

FIGURE 6
Enrichment coefficient of trace elements in different fish teeth.

average of 0.70953). Both the Sr content and $^{87}Sr/^{86}Sr$ isotopic ratio in different marine fish varied in a wide range, as shown in Table 5 and Figure 8. The *Cynoglossus semilaevis* (D_2) had the highest Sr content and range of variation, and also had the highest average $^{87}Sr/^{86}Sr$ ratio, while the *Miichthys miiuy* (D_1) and *Larimichthys crocea* (D_4) had the lowest Sr contents and the least radioactive but biggest fluctuation of $^{87}Sr/^{86}Sr$. The values of the *Scomber japonicus* (D_3) were located in the transition region.

The $^{87}Sr/^{86}Sr$ ratios of the fossil fish teeth ranged from 0.70808 to 0.71075, with an average of 0.70942, close to that of the lake fish teeth but significantly more radioactive than that of the marine fish teeth. Among the fossil fish teeth from different cores, $^{87}Sr/^{86}Sr$ can be ranked as GC03 < GC04 < GC11 from the point of view of minimum, maximum, and average values. The εNd of the fossil fish teeth from the three cores ranged from -8.1 to -2.2 with an average of -4.7, in a sequence of GC04 (-4.2) > GC03 (-4.3) > GC11(-5.7). The fossil fish teeth in the GC03 showed the widest εNd range (-7.0–2.2), while the εNd of GC04 (-6.7–2.2) and GC11 (-8.1–3.9) varied in a relatively narrow range, as shown in Table 6.

5 Discussion

5.1 Enrichment process of trace elements in modern and fossil fish teeth

Except for Mo, W, Zn, and Rb (the contents of which were significantly higher in lake fish teeth), the contents of most elements were higher in the marine fish teeth and further increased by different degrees in the fossil fish teeth after deposition. To evaluate the aggregation capability of the trace elements in the fish teeth during different processes, including the life cycle and post-deposition, M_i/W_i and F_i/M_i were introduced in this study for comparison. M_i/W_i represents the ability of fish teeth to absorb and accumulate trace elements from the water in which they live, while F_i/M_i represents the degree of trace elements diffusion and adsorption to fish teeth after death. Both the amount and the magnitude of trace element enrichment were considered to evaluate the enrichment degree of trace element during the life and after deposition. Then, trace elements were divided into three categories based on their geochemical properties.

TABLE 3 The enrichment coefficient of trace elements (M_i/W_i) in modern marine fish teeth.

Enrichment coefficient	Deficiency /10^{-1}-10^0	Slightly enriched /10^0-10^1	Moderately enriched /10^1-10^2	Highly enriched/ 10^2-10^3	Extremely enriched/>10^3
Elements	Rb	V and Mo	Li, Ti, Fe, As, Cs, and U	Cu, Co, Pb, Ba, W, Zn, Cr, and Sr	Mn, Ga, Zr, Sn, and Th

TABLE 4 The contents and characteristic values of REEs in fossil fish teeth.

ppm		La	Ce	Pr	Nd	Sm	Eu	Gd	Tb	Dy	Y	Ho
GC03 fish teeth	Min	62.10	9.53	14.48	64.30	14.09	3.51	16.94	2.52	17.14	127.30	3.77
	Max	3914.00	726.00	1045.00	4637.00	1040.00	253.60	1160.00	163.70	1035.00	6479.00	200.60
	Ave	1453.94	293.45	380.42	1669.89	386.04	96.35	451.22	66.59	449.41	3016.55	91.80
	SD (n=15)	991.47	226.96	266.07	1182.35	264.79	64.69	298.37	42.02	269.84	1704.76	52.73
GC04 fish teeth	Min	119.00	4.91	22.20	91.00	20.40	5.40	24.90	3.95	29.60	246.00	7.00
	Max	2430.00	448.00	677.00	2990.00	707.00	183.00	817.00	120.00	788.00	4990.00	156.40
	Ave	879.51	111.42	237.15	1038.43	247.39	62.76	293.79	44.06	297.51	2022.33	60.65
	SD (n=15)	677.83	136.53	189.68	831.74	197.74	50.63	231.23	34.46	230.84	1489.51	46.03
GC11 fish teeth	Min	85.20	5.16	27.10	121.20	31.10	7.40	29.90	4.07	24.60	140.00	4.38
	Max	2712.00	1760.00	890.00	3988.00	1026.00	257.50	1169.00	180.80	1205.00	7080.00	238.10
	Ave	1105.50	346.56	341.21	1503.15	375.21	94.57	424.83	64.54	431.91	2630.47	84.58
	SD (n=15)	902.56	471.30	285.11	1261.12	314.67	78.02	345.82	51.39	338.27	2009.59	65.85
The sum of fossil fish teeth	Min	62.10	4.91	14.48	64.30	14.09	3.51	16.94	2.52	17.14	127.30	3.77
	Max	3914.00	1760.00	1045.00	4637.00	1040.00	257.50	1169.00	180.80	1205.00	7080.00	238.10
	Ave	1146.32	250.48	319.59	1403.82	336.21	84.56	389.95	58.40	392.95	2556.45	79.01
	SD (n=45)	880.49	321.50	252.14	1115.33	265.16	65.78	297.05	43.42	285.03	1756.95	55.85
ppm		Er	Tm	Yb	Lu	REE	$(La/Sm)_N$	$(La/Yb)_N$	$(Sm/Yb)_N$	δCe	δEu	δY
GC03 fish teeth	Min	11.28	1.55	10.75	1.72	360.98	0.43	0.13	0.31	0.05	1.05	1.13
	Max	564.30	69.64	464.20	70.58	21718.41	0.72	0.65	1.18	0.23	1.09	1.32
	Ave	276.00	37.65	262.73	39.88	8971.93	0.56	0.39	0.70	0.09	1.07	1.21
	SD (n=15)	148.69	18.74	122.31	17.91	5595.42	0.07	0.13	0.22	0.05	0.01	0.05
GC04 fish teeth	Min	24.20	3.94	30.20	4.60	650.00	0.31	0.16	0.28	0.01	1.04	1.07
	Max	447.00	59.80	410.00	59.30	15282.50	0.85	0.51	1.03	0.09	1.12	1.46
	Ave	183.00	25.29	177.54	26.77	5707.63	0.59	0.36	0.64	0.05	1.07	1.25
	SD (n=15)	134.90	18.26	125.73	18.38	4324.22	0.14	0.09	0.20	0.03	0.02	0.10
GC11 fish teeth	Min	11.60	1.57	11.90	1.43	517.61	0.34	0.22	0.51	0.02	1.05	1.04
	Max	702.00	97.40	674.00	102.40	22074.20	0.63	0.53	1.33	0.26	1.49	1.22

(Continued)

TABLE 4 Continued

ppm		Er	Tm	Yb	Lu	REE	$(La/Sm)_N$	$(La/Yb)_N$	$(Sm/Yb)_N$	δCe	δEu	δY
	Ave	250.97	34.13	237.66	35.30	7960.59	0.43	0.37	0.86	0.10	1.12	1.10
	SD (n=15)	192.91	26.30	181.63	27.33	6399.94	0.07	0.11	0.28	0.09	0.11	0.05
The sum of fossil fish teeth	Min	11.28	1.55	10.75	1.43	360.98	0.31	0.13	0.28	0.01	1.04	1.04
	Max	702.00	97.40	674.00	102.40	22074.20	0.85	0.65	1.33	0.26	1.49	1.46
	Ave	236.66	32.36	225.98	33.98	7546.72	0.53	0.37	0.74	0.08	1.09	1.18
	SD (n=45)	162.00	21.58	146.95	21.85	5554.09	0.12	0.11	0.25	0.06	0.07	0.09

$(La/Sm)_N$, La_N/Sm_N; $(La/Yb)_N$, La_N/Yb_N; $(Sm/Yb)_N$, Sm_N/Yb_N; Ce anomaly (δCe), $2Ce_N/(La_N+Pr_N)$; Eu anomaly (δEu), $2Eu_N/(Sm_N+Gd_N)$; Y anomaly (δY), $2Y_N/(Dy_N+Ho_N)$; "N" represents the normalization value of elements.

1. Type I represents a category of elements that were mainly accumulated in the fish teeth during life with M_i/W_i greatly higher than F_i/M_i, including Sr, Li, Ba, Cr, Mn, Zn, Ga, Sn, Pb, and W. The amount of this type of element was significantly enhanced with a larger magnitude mainly through absorbance by the fish during the life cycle. These elements belong to IA, IIA, IIIA, and IVA groups respectively in the periodic table of elements. The outer electron shells are basically ns^1 (Li, Cr, and Ga), ns^2 (Sr, Ba, Mn, Zn, and W), and ns^2np^2 (Sn and Pb). Their outer electrons are apt to lose and remain stable under oxidation and weak-reduction conditions. It is hypothesized that these elements enter into the organism during life from seawater by ion absorption. Isomorphism with Ca, Mg, Fe, and K may be the reason for their main occurrence in bioapatite.
2. Type II is a group of elements that accumulated in the fish teeth during both the life cycle and post-deposition, including Mo, Rb, U, V, As, Co, Ti, Fe, Cu, Zr, and Th. They exhibited similar degrees of F_i/M_i and M_i/W_i. From the view of magnitude change, the ability of modern fish teeth to absorb these elements from ambient water is similar to that of fossils to adsorb after deposition. These elements belong to the IA, VA, transition elements, and Actinides groups with unsaturated outer electron and/or inner electron shells. Most of them are redox-sensitive elements exhibiting variable valences under different redox conditions. These elements can be accumulated through ion absorption in fish teeth during the life cycle of the fish with a lower valence and can be enriched continuously through adsorption into the fossils in the deep seawater-sediment interface after the deposition period. A higher valence is indicated in the later stage but needs further investigation.
3. Type III represents elements that are enriched in fossils only after deposition, including REEs, Be, Ge, Cd, Sc, Hf, and Tl. They are mainly members of Lanthanides and rare dispersed elements groups with a large atomic radius and strong chemical activity. Except for Be, which has the atomic electronic structure of $1s^22s^2$ with a saturated inner electron shell, the rest have an unsaturated inner electron shell of $nd^{10-n}(nf^{14-n})\ (n+1)s^2$ or unsaturated outer electron shell of $ns^2(n+1)p^{6-(n+1)}$. Ions with a +3 or +4 valence are their main occurrence state. These elements are undetectable in living fish teeth but are highly enriched after fossilization, and, among them, REEs were the most enriched with the highest concentration of 7,546.72 ppm detected in fossil fish teeth in this study. Their large ionic radius and extremely low content in seawater hinder them from entering into the organism and accumulating. However, as the collagen in the fish teeth decomposes during early diagenesis after deposition (Tütken et al., 2008), a large number of pores are generated in the phosphate skeleton, leading to the recrystallization of nanoscale biogenic apatite in the diagenetic fluid and the adsorption of lanthanides from the surrounding

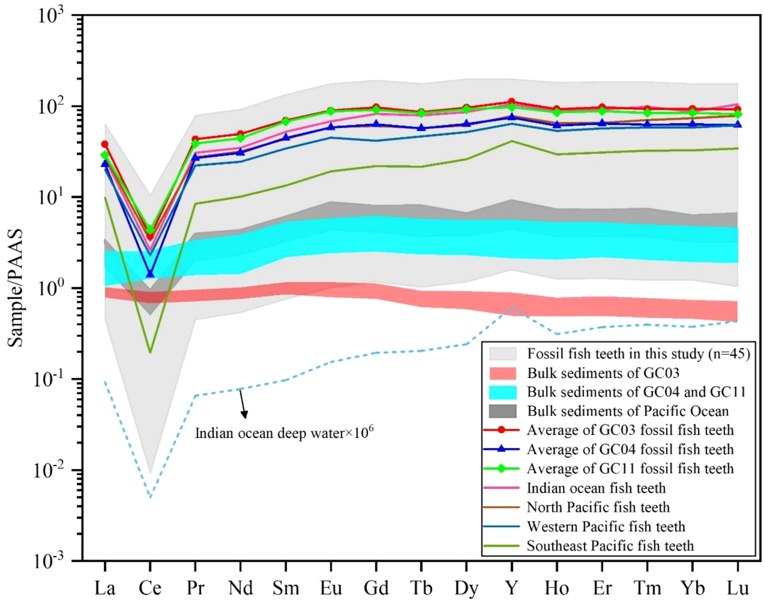

FIGURE 7
REE pattern in fossil fish teeth normalized by PAAS with a comparison with previous studies.

TABLE 5 ^{87}Sr/^{86}Sr, CaO/P_2O_5, and Sr/Ca values of the modern fish teeth.

Sample		CaO (wt.%)	P_2O_5 (wt.%)	CaO/ P_2O_5	Sr (ppm)	Sr/ Ca	^{87}Rb/^{86}Sr	^{87}Sr/^{86}Sr
D_1 (n=15)	Min	29.46	25.13	1.11	624	0.0020	0.00298	0.70633
	Max	48.49	40.30	1.25	1064	0.0023	0.00718	0.70847
	Ave	39.37	33.97	1.16	851	0.0022	0.00408	0.70797
D_2 (n=12)	Min	30.28	25.75	1.02	2294	0.0064	0.00061	0.70830
	Max	47.55	41.16	1.18	3463	0.0077	0.00203	0.70913
	Ave	38.77	34.55	1.12	2747	0.0071	0.00103	0.70895
D_3 (n=8)	Min	32.60	27.40	1.12	1019	0.0031	0.00102	0.70781
	Max	48.15	40.73	1.24	1685	0.0035	0.00179	0.70872
	Ave	38.96	32.90	1.18	1305	0.0033	0.00123	0.70848
D_4 (n=12)	Min	29.49	24.77	1.11	669	0.0022	0.00105	0.70658
	Max	47.55	42.36	1.23	1202	0.0025	0.00378	0.70850
	Ave	37.19	31.89	1.17	890	0.0024	0.00206	0.70801
The sum of marine fish teeth (n=47)	Min	29.46	24.77	1.02	624	0.0020	0.00061	0.70633
	Max	48.49	42.36	1.25	3463	0.0077	0.00718	0.70913
	Ave	38.59	33.41	1.16	1422	0.0037	0.00230	0.70832
QDH_1 (n=13)	Min	35.95	34.47	1.00	359	0.0008	0.00278	0.70918
	Max	46.85	38.51	1.27	540	0.0015	0.00684	0.70973
	Ave	40.40	36.87	1.10	459	0.0012	0.00448	0.70953

TABLE 6 ^{87}Sr/^{86}Sr and ^{143}Nd/^{144}Nd values of the fossil fish teeth.

Sample	^{87}Rb/^{86}Sr	2σ	^{87}Sr/^{86}Sr	2σ	Sr (ppm)	^{147}Sm/^{144}Nd	2σ	^{143}Nd/^{144}Nd	2σ	εNd	Nd (ppm)
GC03-3-05	0.00135	0.00004	0.71043	0.00021	1437	0.15933	0.00018	0.51231	0.00019	-6.2	493
GC03-3-09	0.00393	0.00006	0.70984	0.00013	1365	0.13635	0.00007	0.51251	0.00006	-2.2	2433
GC03-3-10*	0.00753	0.00105	0.70915	0.00018	1338	0.13568	0.00019	0.51208	0.00013	-10.7	2455
GC03-3-11	0.00276	0.00007	0.70892	0.00015	1717	0.13576	0.00008	0.51243	0.00004	-3.9	2124
GC03-3-15	0.00361	0.00003	0.71004	0.00014	1895	0.14113	0.00006	0.51245	0.00004	-3.6	2790
GC03-3-17	0.00205	0.00013	0.70936	0.00048	1868	0.15223	0.00011	0.51248	0.00011	-2.9	948
GC03-3-20	0.00101	0.00004	0.70950	0.00020	1871						
GC03-3-22	0.00146	0.00007	0.70877	0.00021	1792	0.13540	0.00030	0.51227	0.00032	-7.0	1218
GC03-3-23	0.00072	0.00005	0.70875	0.00014	2134						
GC03-3-25	0.00061	0.00008	0.70849	0.00028	1446						
GC03-3-26	0.00203	0.00005	0.70959	0.00018	1697						
GC03-3-30	0.00155	0.00006	0.70913	0.00018	2652						
GC03-3-31	0.00043	0.00017	0.70808	0.00014	2216						
Min	0.00043		0.70808		1365	0.13540		0.51227		-7.0	493
Max	0.00393		0.71043		2652	0.15933		0.51251		-2.2	2790
Ave	0.00179		0.70924		1841	0.14337		0.51241		-4.3	1668
GC04-11	0.00325	0.00063	0.70912	0.00017	1180						
GC04-14	0.00111	0.00003	0.70999	0.00016	1218	0.15504	0.00011	0.51228	0.00008	-6.7	644
GC04-15	0.00547	0.00047	0.71026	0.00015	1419	0.14617	0.00015	0.51238	0.00006	-4.8	2990
GC04-16	0.00186	0.00003	0.70925	0.00020	1352	0.13170	0.00015	0.51241	0.00004	-4.3	1544
GC04-20	0.00026	0.00002	0.70874	0.00018	1750						
GC04-22	0.00010	0.00003	0.70838	0.00016	1489						
GC04-23	0.00218	0.00004	0.71048	0.00017	1024	0.15070	0.00012	0.51252	0.00005	-2.2	1545
GC04-24	0.00269	0.00004	0.71049	0.00027	1490	0.13550	0.00016	0.51247	0.00006	-3.2	1527
GC04-26	0.00155	0.00012	0.70900	0.00035	1362						
GC04-27	0.00089	0.00004	0.70864	0.00014	1650						
GC04-28	0.00074	0.00009	0.70992	0.00012	1782						
GC04-29	0.00210	0.00004	0.71006	0.00015	1357	0.13750	0.00014	0.51240	0.00016	-4.5	1570
GC04-31	0.00125	0.00005	0.70914	0.00020	1520						
GC04-33	0.00063	0.00014	0.70857	0.00016	2618						
GC04-34	0.00047	0.00002	0.70890	0.00015	2059	0.13224	0.00023	0.51243	0.00027	-3.9	1690
Min	0.00010		0.7084		1024	0.1317		0.51228		-6.7	644
Max	0.00547		0.71049		2618	0.15504		0.51252		-2.2	2990
Ave	0.00164		0.70940		1551	0.14126		0.51241		-4.2	1644
GC11-1-04	0.00075	0.00052	0.71075	0.00185	1018						
GC11-1-07	0.01707	0.00305	0.70988	0.00023	1614	0.16670	0.00013	0.51230	0.00009	-6.4	1463
GC11-1-08	0.00162	0.00016	0.70979	0.00030	926.3						
GC11-1-10	0.00222	0.00009	0.70967	0.00036	1196	0.16427	0.00011	0.51231	0.00008	-6.3	1409

(Continued)

TABLE 6 Continued

Sample	$^{87}Rb/^{86}Sr$	2σ	$^{87}Sr/^{86}Sr$	2σ	Sr (ppm)	$^{147}Sm/^{144}Nd$	2σ	$^{143}Nd/^{144}Nd$	2σ	εNd	Nd (ppm)
GC11-2-08	0.00887	0.00064	0.70931	0.00025	1379						
GC11-2-20	0.00632	0.00005	0.70954	0.00015	1467	0.15849	0.00025	0.51236	0.00003	-5.2	3988
GC11-2-24	0.00089	0.00004	0.70970	0.00021	1244	0.14988	0.00012	0.51240	0.00004	-4.5	1930
GC11-2-25	0.00136	0.00003	0.70863	0.00017	1697						
GC11-2-29	0.00167	0.00004	0.70996	0.00015	1867	0.15318	0.00030	0.51222	0.00016	-8.1	1700
GC11-2-34	0.00128	0.00003	0.71000	0.00013	1480						
GC11-2-42	0.00354	0.00005	0.70920	0.00015	2061	0.13788	0.00006	0.51243	0.00004	-3.9	2970
GC11-2-43*	0.08183	0.00593	0.71467	0.00372	1274	0.14355	0.00015	0.51243	0.00005	-3.9	1856
GC11-2-47	0.00043	0.00004	0.70922	0.00021	1202						
Min	0.00043		0.70863		926	0.13788		0.51222		-8.1	1409
Max	0.01707		0.71075		2061	0.16670		0.51243		-3.9	3988
Ave	0.00383		0.70964		1429	0.15507		0.51234		-5.7	2243
Min of the sum	0.00010		0.70808		926	0.13170		0.51222		-8.1	493
Max of the sum	0.01707		0.71075		2652	0.16670		0.51252		-2.2	3988
Ave of the sum	0.00236		0.70942		1603	0.14629		0.51239		-4.7	1841

*Denotes that two of the fossil fish teeth samples have abnormal values: GC11-2-43 had the highest value and standard error of $^{87}Sr/^{86}Sr$ (0.71467 ± 0.00372) with a very high εNd value (-3.9), while GC03-3-10 had the lowest $^{143}Nd/^{144}Nd$ value (0.51208 ± 0.00013) and a less radiogenic $^{87}Sr/^{86}Sr$ (0.70915). The presence of weathering products in the porous teeth may be the reason as discussed and data from the two samples were then rejected according to Zhang et al. (2023). The eigenvalue values were then recalculated without the two outliers.

environment with other rare dispersed elements (Trueman et al., 2004). This process occurs under oxidizing or suboxidizing environments at the deep seawater-sediment interface, accompanied by low sedimentation rates and strong adsorption, resulting in the extreme accumulation of REEs in particular.

It should be noted that F in fossil fish teeth was much higher than that in modern fish teeth with 0.00%–1.05%, which can be attributed to the transformation of hydroxyapatite into hydroxyfluorapatite after deposition in which the hydroxide is replaced by F. This transformation was indicated to be the main factor accelerating the adsorption of Nd, resulting in 3 to 6 orders of

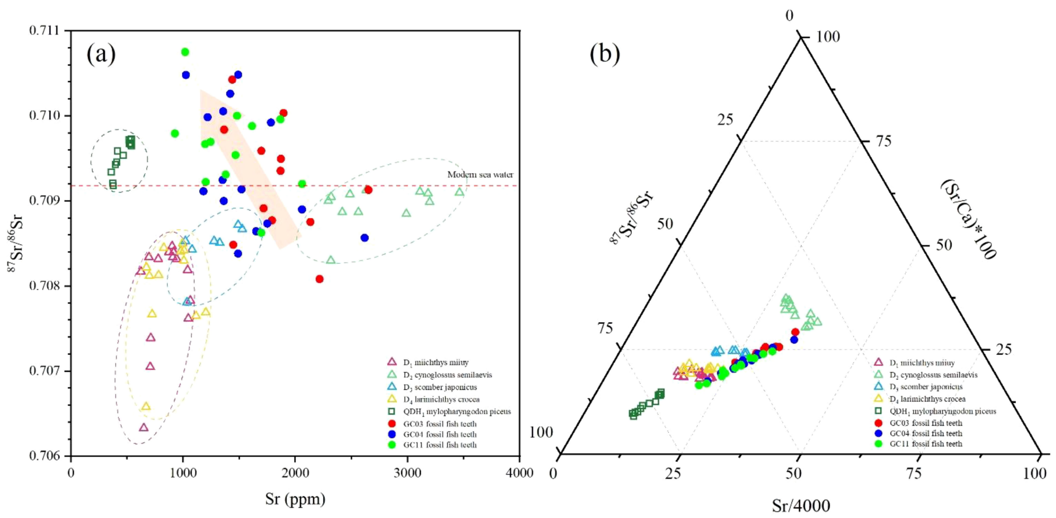

FIGURE 8
(a) $^{87}Sr/^{86}Sr$-Sr of fish teeth; **(b)** Sr/Ca-Sr-$^{87}Sr/^{86}Sr$ triangular diagram of fish teeth.

magnitude more Nd in fossil fish teeth than in living fish teeth (Wright et al., 1984; Shaw and Wasserburg, 1985; Staudigel et al., 1985). The extreme enrichment of REE in bio-apatite is related to ion exchange with $REE^{3+}+Na^{+}\rightarrow 2Ca^{2+}$; $REE^{3+}+Si^{4+}\rightarrow Ca^{2+}+P^{5+}$. It has been shown that biological apatite is composed of elongated nanocrystals arranged with hexagonal hydroxyapatite cross sections, with large porosity and extremely high specific surface area, which is conducive to REE adsorption. In addition, Si-rich regions appear along the nanoboundary, showing element exchange along the mineral nanocrystal boundary, confirming the presence of Na, Si, Ce, and Y in the biological apatite nanocrystals, and indicating that atoms heavier than Ca (Ln, such as Ce and Y) are substituted into the lattice, with weaker peaks associated with the exchange of lighter Na atoms (Liao et al., 2019a).

In general, the occurrence of trace elements in fish teeth is influenced by the geochemical properties of elements, the crystal structure of bio-apatite, and the redox conditions in different processes. This can be shown in a two-stage three-classification model, as shown in Figure 9.

5.2 Geochemical significance of Sr/Ca-$^{87}Sr/^{86}Sr$-Sr

As a highly enriched trace element in modern fish (M_i/W_i=293.6, Figure 6), Sr is indicated to be mainly absorbed by the fish teeth during life and is slightly enriched by recrystallization exchange after deposition (with the smallest F_i/M_i of 1.13, Figure 6). Previous research has proved that the deposition of some trace elements in otolith is related to the history of fish migration in addition to their contents in water and the environmental temperature (Beck et al., 1992; Izzo et al., 2018; Hüssy et al., 2021; Arai and Kimura, 2022). In this study, the much higher Sr content in the marine fish teeth (1425.18 ppm) than lake fish teeth (455.10 ppm) is consistent with the large difference of Sr content in seawater (7.88 ppm) and in rivers (0.09 ppm) (Anadón et al., 2002). In addition, the Sr/Ca ratio was significantly positively correlated with Sr content in fish teeth (R^2 = 0.87) (Figure 5b), but differences in Sr/Ca and $^{87}Sr/^{86}Sr$ were also found among different modern marine fish species (Figure 8). It is reasonable to assume that element composition (especially Sr and Ca) was also recorded in the fish teeth, similar to those in the otolith (Avigliano et al., 2018; Bock et al., 2017). This means that in the process of material exchange between fish and the external environment, some trace elements are continuously ingested into the fish, and after a series of metabolisms and circulations, finally also deposited in fish teeth.

In addition, the observed lower $^{87}Sr/^{86}Sr$ of marine fish teeth (0.70832) than that of lake fish teeth (0.70953) (Figure 8) is consistent with the difference of $^{87}Sr/^{86}Sr$ between seawater [modern seawater average $^{87}Sr/^{86}Sr$=0.70917 (McArthur et al., 2020)] and inland freshwater [world river average $^{87}Sr/^{86}Sr$=0.71190 (Palmer and Edmond, 1989)], while the $^{87}Sr/^{86}Sr$ of the lower reaches of Yangtze River (Datong station) was 0.71063 (Luo et al., 2014). Both the $^{87}Sr/^{86}Sr$ of the lake fish teeth and marine fish teeth were lower than the ambient waters, and the $^{87}Sr/^{86}Sr$ ratios of all the fish teeth were lower than that of modern seawater (Figure 8). It was noted that the Sr/Ca and $^{87}Sr/^{86}Sr$ of D_1 and D_4 overlapped greatly, while D_2 exhibited significantly higher Sr/Ca and $^{87}Sr/^{86}Sr$, and D_3 was located in the transition region of Sr/Ca-$^{87}Sr/^{86}Sr$ (Figures 5b, 8). The significantly different Sr/Ca-$^{87}Sr/^{86}Sr$ among these marine fish teeth should be closely related to their different migration habit. As mentioned, D_1, D_3, and D_4 usually migrate from deep water to nearshore for relatively long distances, thus recording a chemical composition and $^{87}Sr/^{86}Sr$ ratios in a wide range. In comparison, due

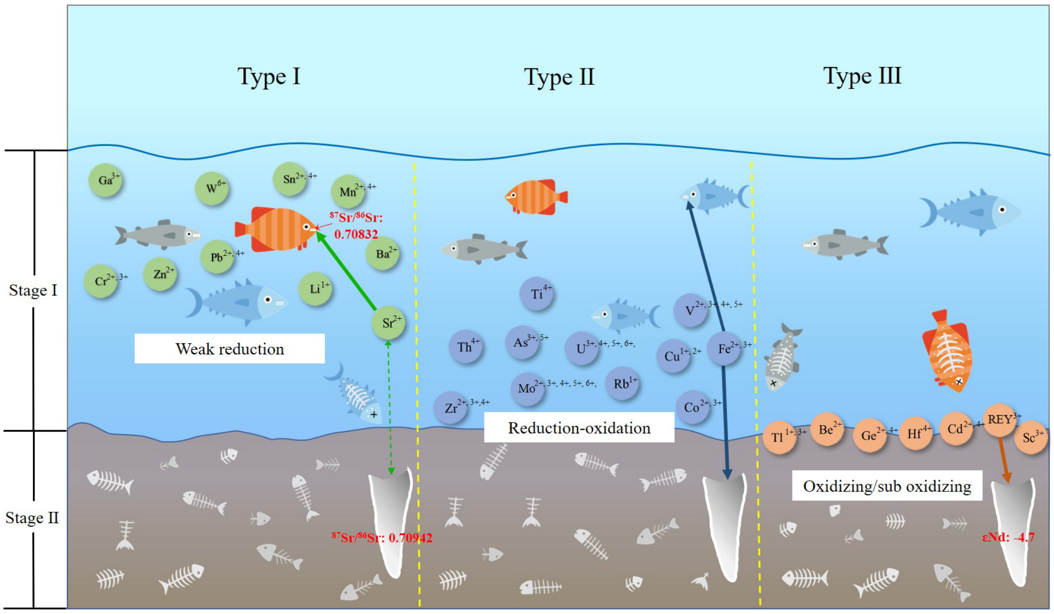

FIGURE 9
Three different enrichment phases of trace elements in fish teeth.

TABLE 7 Comparison of Sr-Nd isotopes and different components in fossil fish teeth from different sea areas.

Area	Site	Sample	Depth/ mbsf	Age/Ma	$^{87}Sr/^{86}Sr$	$^{143}Nd/^{144}Nd$	εNd	Reference
Indian Ocean	Site 757	Fossil fish teeth	3.71–136.8	0.52–35.92	**0.708527** (0.707758–0.709115, n=33)	**0.512313** (0.512233–0.512396, n=30)	**-6.3** (-7.9–4.7, n=30)	Martin and Scher, 2004; Martin and Scher, 2006; Gourlan et al., 2008
		Fossil foraminifera	6.42–141.1	0.90–36.81	**0.708488** (0.707654–0.709130, n=47)	**0.512319** (0.512238–0.512402, n=52)	**-6.2** (-7.8–4.6, n=52)	
		Pore water	2.73–108.25	0.38–28.00	**0.708566** (0.708124–0.709055, n=8)			
	Site 756	Fossil foraminifera	0.02–109.5	0.03-31.37		**0.512285** (0.512210–0.512507, n=84)	**-6.9** (-8.4–2.6, n=84)	Houedec et al., 2012
		Detrital fraction	1.28–100.7	1.98–30.46	**0.716180** (0.705503–0.727734, n=15)	**0.512121** (0.511930–0.512543, n=15)	**-10.0** (-14.0–1.8, n=15)	
	Site 762	Fossil foraminifera	6.91–209.86	0.48–35.01		**0.512224** (0.512074–0.512396, n=20)	**-8.1** (-11.0–4.7, n=20)	
		Detrital fraction	20.94–209.86	1.47–35.01		**0.511762** (0.511510–0.512150, n=13)	**-17.1** (-22.0–9.5, n=13)	
	Site 758	Fossil foraminifera	0.08–289.8	0.004–23.39		**0.512191** (0.512110–0.512250, n=25)	**-8.6** (-10.3–7.1, n=25)	Gourlan et al., 2008
	Site 707	Fossil foraminifera	1.74–127.05	0.3–17.2		**0.512332** (0.512239–0.512417, n=31)	**-6.0** (-7.8–4.3, n=31)	
	SS663	Silicates of Fe-Mn crust		0.7–24.4	**0.713751** (0.708305–0.721476, n=6)	**0.512124** (0.511987–0512241, n=6)	**-10.0** (-12.7–7.7, n=6)	Banakar et al., 2003
	DODO 108P	Fossil fish teeth		36.8–37.8	**0.707839** (± 0.000032)	**0.512117** (± 0.000057)	**-10.2**	Staudigel et al., 1985
	DODO 111P	Fossil fish teeth		21.5–26.0	**0.708504** (± 0.000033)	**0.512185** (± 0.000013)	**-8.8**	
	SWCI	Silicates of sediment	Core top	Late Holocene to modern	**0.716660** (0.714860–0.719120, n=6)	**0.51176** (0.51118–0.51215, n=6)	**-17.0** (-28.3–9.3, n=6)	Subha Anand et al., 2019
	CIR	Silicates of sediment	Core top	Late Holocene to modern	**0.709440** (0.708100–0.710270, n=13)	**0.51222** (0.51214–0.51244, n=13)	**-8.0** (-9.6–3.6, n=13)	
	SWIR	Silicates of sediment	Core top	Late Holocene to modern	**0.713570** (0.705270–0.724930, n=12)	**0.51240** (0.51209–0.51262, n=5)	**-4.6** (-10.5–0.3, n=5)	
	ANT	Silicates of sediment	Core top	Late Holocene to modern	**0.752460** (0.728660–0.778490, n=7)	**0.51127** (0.51085–0.51169, n=7)	**-26.5** (-34.7–18.3, n=6)	
	GC03	Fossil fish teeth	0.00–0.20	2.5Ma–1.3Ma to modern*	**0.709240** (0.708080–0.710430, n=12	**0.51241** (0.51227–0.51251, n=6)	**-4.3** (-7.0–2.2, n=6)	In this study
	GC04	Fossil fish teeth	0.00–0.35	4.4Ma–2.3Ma to modern*	**0.709400** (0.708400–0.710490, n=15)	**0.51241** (0.51228–0.51252, n=7)	**-4.2** (-6.7–2.2, n=7)	
	GC11	Fossil fish teeth	0.00–0.20	2.5Ma–1.3Ma to modern*	**0.709640** (0.708630–0.710750, n=12)	**0.51234** (0.51222–0.51243, n=6)	**-5.7** (-8.1–3.9, n=6)	
Pacific Ocean	Site 807	Fossil fish teeth	149.9–349.9	5.96–13.13	**0.708854** (0.708792–0.708930, n=7)			Martin and Scher, 2004; Gourlan et al., 2008
		Fossil foraminifera	64.3–349.9	3.25–13.13	**0.708905** (0.708975–0.709045, n=12)	**0.512468** (0.512930–0.512541, n=15)	**-3.3** (-4.8–1.9, n=15)	

(Continued)

TABLE 7 Continued

Area	Site	Sample	Depth/ mbsf	Age/Ma	$^{87}Sr/^{86}Sr$	$^{143}Nd/^{144}Nd$	εNd	Reference
		Pore water	13.35–395.1	0.98–14.5	**0.708893** (0.708633–0.709042, n=6)			
	P57	Phosphate solution	2.7–7.2	0–25	**0.708538** (0.708296–0.708856, n=20)	**0.512334** (0.512309–0.512350, n=19)	**-5.9** (-6.4–5.6, n=19)	Ren et al., 2022
		Non-phosphate residue	2.7–7.2	0–25	**0.710484** (0.709122–0.712120, n=10)	**0.512306** (0.512260–0.512325, n=19)	**-6.5** (-7.4–6.1, n=19)	
	GC062	Fossil fish teeth	0.0–8.0	<16		**0.512325** (0.512021–0.512565, n=48)	**-6.1** (-12.0–6.1, n=48)	Deng et al., 2022
Atlantic sector of the Southern Ocean	Site 689	Fossil fish teeth	60.59–182.97	17.91–46.21	**0.707927** (0.707794–0.708251, n=31)	**0.512190** (0.512133–0.512246, n=79)	**-8.6** (-9.8–7.7, n=79)	Martin and Scher, 2004; Scher and Martin, 2006
		Fossil foraminifera	66.62–182.97	20.06–46.21	**0.707836** (0.707717–0.708421, n=26)			
		Pore water	49.00–164.45	12.37–42.07	**0.708476** (0.708220–0.708730, n=5)			
	Site 1090	Fossil fish teeth	71.79–403.005	16.09–43.007	**0.708065** (0.707687–0.708654, n=114)	**0.512261** (0.512184–0.512359, n=242)	**-7.4** (-8.9–5.5, n=242)	
		Fossil foraminifera	71.79–401.22	16.09–40.62	**0.708140** (0.707704–0.708727, n=92)			
		Pore water	80.34–405.74	17.52–40.84	**0.707934** (0.707645–0.708332, n=27)			

SWCI, Southwest coast of India; CIR, Central Indian Ridge; SWIR, Southwest Indian Ridge; ANT, Antarctica.
*Means the ages were calculated with the deposition rate of 0.8–1.5 mm/Ka.
The bold values in the table represent average values.

to its lack of nearshore migration, D_2 has narrow $^{87}Sr/^{86}Sr$ ratios. A trigonometric diagram of Sr/Ca- $^{87}Sr/^{86}Sr$-Sr was then created to distinguish different aquatic environments, as shown in Figure 8.

Previous studies have pointed out that andesite on Taiwan Island ($^{87}Sr/^{86}Sr$=0.70489) and basalt on the coast of Zhejiang and Fujian provinces ($^{87}Sr/^{86}Sr$=0.70805) are important material sources for the ECS (Mi et al., 2017). Moreover, the Okinawa Trough, located at the eastern boundary of the ECS, is tectonically active with frequent volcanism. The acidic volcanic rock in the north-central trough has $^{87}Sr/^{86}Sr$ ranging from 0.70406 to 0.70544 (Huang et al., 2006). These potential sources of Sr isotopes may result in the less radioactive $^{87}Sr/^{86}Sr$ composition of the regional seawater of the ECS and are recorded in the fish teeth during migration. $^{87}Sr/^{86}Sr$ in the lake fish teeth varied in a narrow range but was higher than the $^{87}Sr/^{86}Sr$ of carbonate rocks in the Yangtze River Basin, varying from 0.70800 to 0.70900 (Chetelat et al., 2008), also suggesting that the weathering of exposed marine carbonate rocks in the area around Qiandaohu Lake may result in relatively low $^{87}Sr/^{86}Sr$ in the lake water and subsequent adsorbed to fish teeth.

In comparison, the correlation between Sr/Ca-Sr was more significant in the fossil fish teeth (R^2 = 0.98, Figure 5b), and similar consistent characteristics could be found in $^{87}Sr/^{86}Sr$ (Figure 8). In the case of the main component remaining unchanged under an open system, a strong replacement of Sr after deposition accompanies the significantly strong correlation between Sr/Ca-Sr. However, it is interesting that a negative correlation of Sr-$^{87}Sr/^{86}Sr$ was observed for the fossil fish teeth. It was proved that Sr changed because of teeth recrystallization and exchange with pore fluid Sr^{2+} during burial and diagenesis (Martin and Scher, 2004). In this process, the interference of the Sr isotope from different sources with the original Sr isotope in fish teeth cannot be ignored.

5.3 Paleoceanographic record in fossil fish teeth and its uncertainty

The average $^{87}Sr/^{86}Sr$ in fossil fish teeth from the CIOB is 0.70942 (from 0.70808 to 0.71075), significantly more radiogenic than the ancient and modern seawater (increasing from 0.70770 at about 40 Ma to 0.70920 at present) (McArthur et al., 2001). Previous studies have indicated that the Sr isotope may be recrystallized and exchanged with Sr in pore water after deposition under the influence of diagenesis, which affected the original Sr isotope record (Martin and Scher, 2004). The $^{87}Sr/^{86}Sr$ of the fossil fish teeth in the 2-m cores from the CIOB was higher than the fossil fish teeth ($^{87}Sr/^{86}Sr$=0.70853) and foraminifera ($^{87}Sr/^{86}Sr$=0.70849) buried deep in the Indian Ocean but was very close to the $^{87}Sr/^{86}Sr$ of the silicate components ($^{87}Sr/^{86}Sr$=0.70944) in the surface sediments of the CIR and has a strong terrigenous property (Table 7). The results of chemical leaching experiments from Western Pacific sediments show that although the $^{87}Sr/^{86}Sr$ of phosphate components ($^{87}Sr/^{86}Sr$=0.70830–0.70917) is between the range of seawater since 25 Ma, it does not decrease with the increase of depth, which also indicates a strong terrigenous attribution (Ren et al., 2022).

It is interesting that the corresponding lower εNd under the influence of terrigenous debris was not observed in the fossil fish teeth, and, on the contrary, the εNd was more radioactive with an average of -4.7 (from -8.1– -2.2) (Table 7). It was also more radioactive than the Antarctic circumpolar current (ACC) and the Indian Ocean mean water [εNd=-7–9, Albarède et al. (1997)] recorded by iron manganese oxides in the seabed, and appears to be very close to the Pacific Ocean [εNd=-5–4, Ling et al. (2005)] and the silicate components in the surface sediments of the SWIR [εNd=-4.6, Subha Anand et al. (2019)], indicating the uncertainty of the paleoceanographic information record in the samples of this study.

Recent studies have found that REEs in pore water near the sediment-seawater interface may be an important source of rare earth elements in rare earth-rich sediments (Liao et al., 2019b; Deng et al., 2022). Bioapatite can obtain REEs from terrigenous detrital deposits through pore water (Elderfield and Pagett, 1986) and the Nd isotope of biological apatite in volcanic detrital deposits has obvious volcanic origin characteristics (Zhao et al., 2013). A study found that εNd in fossil fish teeth was unevenly distributed and varied widely, gradually increasing from the root to the tip of fish teeth and was significantly different from the seawater (Deng et al., 2022). An inference from this is that the original εNd values of bioapatite in deep-sea sediment may be altered by pore water with high Nd concentrations and low εNd values during diagenesis. The difference was also found in this study, but the trend was reversed so that the εNd of the fossil fish teeth was more radioactive than the Indian Ocean water. This may be related to the same high Nd concentrations but different εNd of pore water under the influence of sediment components.

For the sediment input of the CIOB, a higher ^{87}Sr/^{86}Sr ratio and lower εNd near Antarctica indicate old granitic rocks as the source, and the opposite is observed in sediments from the Central and the Southwest Indian Ridges, indicating seafloor spreading and mid-ocean ridge hydrothermal activity as the source (Subha Anand et al., 2019). It is noteworthy that the ^{87}Sr/^{86}Sr ratio increases along with decreasing Sr content in the fossil fish teeth from GC03 (0.70924) and GC04 (0.70940) to GC11 (0.70964). It is possible that the GC11 core, at a lower latitude than the GC03 and GC04 cores, was more influenced by continental detritus from Antarctica sources with high ^{87}Sr/^{86}Sr. Furthermore, high field strength elements Hf and Zr, large ion lithophile element Sr, and rare earth elements exhibited a decreasing trend in the fossil fish teeth with GC03>GC04>GC11 (Table 2), which indicates a weakened terrigenous signal from GC11 and GC04 to GC03. It is reasonable to speculate that fine terrestrial debris with high ^{87}Sr/^{86}Sr may enter the fine pores of fish teeth or through exchange of Sr isotopes at the microscopic level after deposition but with minor impact on the Sr content. If so, fossil fish teeth may preserve the influence from enhanced continental weathering signal and prove the long diagenesis influence after deposition (Martin and Scher, 2004).

As for the significantly more radioactive εNd, it may be closely related to the release of Nd from volcanic hydrothermal components in sediments into pore water. While cores GC03 and GC04 were less affected by Antarctic continental debris, they received more from seafloor spreading and mid-ocean ridge hydrothermal activity (Subha Anand et al., 2019), and the radioactive εNd of these materials may have been absorbed by fish teeth through pore water after deposition. This means that fossil fish teeth may also preserve the influence from volcanic hydrothermal weathering signal and the influence is multi-factor controlled. In general, the suspected sources or continuous absorption of Sr and REEs from pore water could occur, which may cast doubt on the reliability of fish teeth fossils as valid records of deep-sea environments in Earth's history over millions of years. The fractionation of Sr-Nd isotopes in fish teeth and the related diagenetic change after burial are worthy of further study.

6 Conclusion

To further explore the potential capability of trace elements, ^{87}Sr/^{86}Sr, and εNd in modern and fossil fish teeth to be indicators in aquatic environments, material sources tracing, and paleoceanography reconstruction, the mineralogy, major and trace elements, and isotopic composition of fossil fish teeth from the Central Indian Ocean and modern marine and lake fish teeth from East China Sea and Qiandaohu Lake in eastern China were examined and compared. The main conclusions we reached are as follows:

1. According to the element contents in living and fossil fish teeth, the Mi/Wi and Fi/Mi ratios were calculated, which indicated that elements enter into fish teeth during the life cycle of the organism and/or into fossil fish teeth after deposition. Three types of trace elements were classified according to their different manners of enrichment. Type I: Sr, Li, Ba, Cr, Mn, Zn, Ga, Sn, Pb, and W, belonging to the IA, IIA, IIIA and IVA groups, respectively, in the periodic table of elements, can be easily oxidized and accumulate during life cycle into the fish teeth through absorption and remain stable under the oxidation and weak-reduction conditions of the modern marine environment. Type II: Mo, Rb, U, V, As, Co, Ti, Fe, Cs, Cu, Zr, and Th, belonging to the IA, VA, transition elements, and Actinides groups, exhibit variable valence under different redox conditions. These elements can be enriched through ion absorption in fish teeth during the life cycle with a lower valence, and also can be aggregated continuously through adsorption into fish teeth with a high valence in the deep seawater-sediment interface after deposition. Type III: REEs, Be, Ge, Cd, Sc, In, Hf, Tl, and Bi, mainly members of Lanthanides and rare dispersed elements groups with a large atomic radius and strong chemical activity. These elements are enriched only after deposition with a large number of pores generated in the phosphate skeleton, leading to the recrystallization of nanoscale biogenic apatite in the diagenetic fluid and the adsorption of lanthanides from the surrounding environment with other rare dispersed elements. It is indicated the enrichment processes are closely associated with the geochemical properties of these elements, the isomorphism and mineral crystal structure, and the redox environments.
2. The Sr/Ca and ^{87}Sr/^{86}Sr in the modern fish teeth reflect the influence of different aquatic environments and fish migration.

The generally lower $^{87}Sr/^{86}Sr$ in the modern fish teeth may be affected by the contribution of Sr isotopes from regional sediment sources. As for the differentiation of Sr/Ca and $^{87}Sr/^{86}Sr$ in the modern fish teeth, it is mainly related to the migration of the fish. Changes in geochemical elements and Sr isotope composition of swimming fish between seawater and freshwater during migration have been recorded in fish teeth.

3. The more radioactive $^{87}Sr/^{86}Sr$ ratios in fossil fish teeth than in modern seawater reflect the influence of terrigenous sources on fossil fish teeth. The fact that there was increased $^{87}Sr/^{86}Sr$ in the fossil fish teeth from GC03, GC04 and GC11 suggests more Sr isotope contributions from Antarctic continental detritus. Furthermore, the higher εNd values of the fossil fish teeth than those of the Indian Ocean may reflect the effect of pore water on the enrichment of REEs in fossil fish teeth after deposition. The release of radioactive εNd from the mantle-derived volcanic hydrothermal components into pore water may be a possible explanation but needs further study.

Data availability statement

The original contributions presented in the study are included in the article/supplementary material. Further inquiries can be directed to the corresponding author.

Ethics statement

The manuscript presents research on animals that do not require ethical approval for their study.

Author contributions

XZ: Data curation, Formal analysis, Methodology, Software, Validation, Visualization, Writing – original draft, Writing – review & editing. ZX: Conceptualization, Data curation, Formal analysis, Funding acquisition, Methodology, Project administration, Resources, Supervision, Writing – original draft, Writing – review & editing. KZ: Data curation, Methodology, Resources, Writing – original draft. MH: Data curation, Investigation, Writing – original draft. MY: Data curation, Investigation, Writing – original draft. ZL: Data curation, Writing – original draft. ZQ: Methodology, Investigation, Writing – original draft. YL: Data curation, Formal analysis, Methodology, Writing – original draft.

Funding

The author(s) declare that financial support was received for the research and/or publication of this article. This study was supported by the National Natural Science Foundation of China (41773005) and the 13th Five-Year Plan Project for the Investigation and Development of International Marine Resources (DY135-R2-1-01).

Acknowledgments

We thank Prof. Songming Zhu and Zhangying Ye of the College of Biosystems Engineering and Food Science, Zhejiang University of China for the lake fish teeth samples for this study, and Prof. Jingsong Bao of College of Agriculture and Biotechnology, Zhejiang University of China for providing experiment supervision.

Conflict of interest

The authors declare that the research was conducted in the absence of any commercial or financial relationships that could be construed as a potential conflict of interest.

Generative AI statement

The author(s) declare that no Generative AI was used in the creation of this manuscript.

Publisher's note

References

Albarède, F., Goldstein, S. L., and Dautel, D. (1997). The neodymium isotopic composition of manganese nodules from the Southern and Indian oceans, the global oceanic neodymium budget, and their bearing on deep ocean circulation. *Geochimica Cosmochimica Acta* 61, 1277–1291. doi: 10.1016/S0016-7037(96)00404-8

Anadón, P., Gliozzi, E., and Mazzini, I. (2002). Paleoenvironmental reconstruction of marginal marine environments from combined paleoecological and geochemical analyses on ostracods. *Ostracoda: Appl. quaternary Res.* 131, 227–247. doi: 10.1029/131GM12

Arai, T., and Kimura, S. (2022). Spatiotemporal variability of trace elements fingerprints in otoliths of Japanese eel (Anguilla japonica) and its use in tracing geographic origin. *Biology* 11, 1733. doi: 10.3390/biology11121733

Avigliano, E., Miller, N., and Volpedo, A. V. (2018). Silversides (Odontesthes bonariensis) reside within freshwater and estuarine habitats, not marine environments. *Estuarine Coast. Shelf Science.* 205, 123–130. doi: 10.1016/j.ecss.2018.03.014

Banakar, V. K., Galy, A., Sukumaran, N. P., Parthiban, G., and Volvaiker, A. Y. (2003). Himalayan sedimentary pulses recorded by silicate detritus within a ferromanganese crust from the Central Indian Ocean. *Earth Planetary Sci. Lett.* 205 (3-4), 337–348. doi: 10.1016/S0012-821X(02)01062-2

Beck, J. W., Edwards, R. L., Ito, E., Taylor, F. W., Recy, J., Rougerie, F., et al. (1992). Sea-surface temperature from coral skeletal strontium/calcium ratios. *Science* 257, 644–647. doi: 10.1126/science.257.5070.644

Bi, D., Shi, X., Huang, M., Yu, M., Zhou, T., Zhang, Y., et al. (2021). Geochemical and mineralogical characteristics of deep-sea sediments from the western North Pacific Ocean: Constraints on the enrichment processes of rare earth elements. *Ore Geology Rev.* 138, 104318. doi: 10.1016/j.oregeorev.2021.104318

Bijvelds, M. J., van der Velden, J. A., Kolar, Z. I., and Flik, G. (1998). Magnesium transport in freshwater teleosts. *J. Exp. Biol.* 201, 1981–1990. doi: 10.1242/jeb.201.13.1981

Bock, L. R., Whitledge, G. W., Pracheil, B., and Bailey, P. (2017). Relationships between water and paddlefish Polyodon spathula dentary elemental and stable-isotopic signatures: potential application for reconstructing environmental history. *J. Fish Biol.* 90, 595–610. doi: 10.1111/jfb.2017.90.issue-2

Bouvier, A., Vervoort, J., and Patchett, P. (2008). The Lu-Hf and Sm-Nd isotopic composition of CHUR: Constraints from unequilibrated chondrites and implications for the bulk composition of terrestrial planets. *Earth Planetary Sci. Lett.* 273, 48–57. doi: 10.1016/j.epsl.2008.06.010

Chetelat, B., Liu, C. Q., Zhao, Z. Q., Wang, Q. L., Li, S. L., Li, J., et al. (2008). Geochemistry of the dissolved load of the Changjiang Basin rivers: anthropogenic impacts and chemical weathering. *Geochimica Cosmochimica Acta* 72, 4254–4277. doi: 10.1016/j.gca.2008.06.013

Das, P., Iyer, S. D., and Kodagali, V. N. (2007). Morphological characteristics and emplacement mechanism of the seamounts in the Central Indian Ocean Basin. *Tectonophysics* 443, 1–18. doi: 10.1016/j.tecto.2007.08.002

Deng, Y., Guo, Q., Liu, C., He, G., Cao, J., Liao, J., et al. (2022). Early diagenetic control on the enrichment and fractionation of rare earth elements in deep-sea sediments. *Sci. Adv.* 8, eabn5466. doi: 10.1126/sciadv.abn5466

Dyment, J. (1993). Evolution of the Indian ocean triple junction between 65 and 49 ma (anomalies 28 to 21). *J. Geophysical Research: Solid Earth.* 98, 13863–13877. doi: 10.1029/93JB00438

Elderfield, H., and Pagett, R. (1986). Rare earth elements in ichthyoliths: variations with redox conditions and depositional environment. *Sci. Total Environment.* 49, 175–197. doi: 10.1016/0048-9697(86)90239-1

Elderfield, H., Upstill-Goddard, R., and Sholkovitz, E. R. (1990). The rare earth elements in rivers, estuaries, and coastal seas and their significance to the composition of ocean waters. *Geochimica Cosmochimica Acta* 54, 971–991. doi: 10.1016/0016-7037(90)90432-K

Gourlan, A. T., Meynadier, L., and Allègre, C. J. (2008). Tectonically driven changes in the Indian Ocean circulation over the last 25 Ma: Neodymium isotope evidence. *Earth Planetary Sci. Lett.* 267 (1-2), 353–364. doi: 10.1016/j.epsl.2007.11.054

Grandjean, P., Cappetta, H., Michard, A., and Albarede, F. (1987). The assessment of REE patterns and ^{143}Nd/^{144}Nd ratios in fish remains. *Earth Planetary Sci. Letters.* 84, 181–196. doi: 10.1016/0012-821X(87)90084-7

Hein, J. R., Conrad, T., Mizell, K., Banakar, V. K., Frey, F. A., and Sager, W. W. (2016). Controls on ferromanganese crust composition and reconnaissance resource potential, Ninetyeast Ridge, Indian Ocean. *Deep Sea Res. Part I: Oceanographic Res. Papers.* 110, 1–19. doi: 10.1016/j.dsr.2015.11.006

Houedec, S. L., Meynadier, L., and Allègre, C. J. (2012). Nd isotope systematics on ODP Sites 756 and 762 sediments reveal major volcanic, oceanic and climatic changes in South Indian Ocean over the last 35 Ma. *Earth Planetary Sci. Lett.* 327-328, 29–38. doi: 10.1016/j.epsl.2012.01.019

Huang, P., Li, A., Hu, N., Fu, Y., and Ma, Z. (2006). Isotopic feature and uranium dating of the volcanic rocks in the Okinawa Trough. *Sci. China Ser. D.* 49, 375–383. doi: 10.1007/s11430-006-0375-8

Hughes, J. M., and Rakovan, J. (2002). The crystal structure of apatite, Ca5(PO4)3(F, OH, Cl). *Rev. mineralogy geochemistry.* 48, 1–12. doi: 10.2138/rmg.2002.48.1

Hüssy, K., Limburg, K. E., De Pontual, H., Thomas, O. R., Cook, P. K., Heimbrand, Y., et al. (2021). Trace element patterns in otoliths: the role of biomineralization. *Rev. Fisheries Sci. Aquaculture.* 29, 445–477. doi: 10.1080/23308249.2020.1760204

Ingram, B. L. (1995). High-resolution dating of deep-sea clays using Sr isotopes in fossil fish teeth. *Earth Planetary Sci. Letters.* 134, 545–555. doi: 10.1016/0012-821X(95)00151-2

Iyer, S. D. (1991). Comparison of internal features and microchemistry of ferromanganese crusts from the Central Indian Basin. *Geo-marine letters.* 11, 44–50. doi: 10.1007/BF02431054

Iyer, S. D. (2005). Evidences for incipient hydrothermal event (s) in the Central Indian Basin: a review. *Acta Geologica Sinica-English Edition.* 79, 77–86. doi: 10.1111/j.1755-6724.2005.tb00869.x

Iyer, S. D., Mascarenhas-Pereira, M. B. L., and Nath, B. N. (2007). Native aluminium (spherules and particles) in the Central Indian Basin sediments: Implications on the occurrence of hydrothermal events. *Mar. Geology.* 240, 177–184. doi: 10.1016/j.margeo.2007.02.004

Izzo, C., Reis-Santos, P., and Gillanders, B. M. (2018). Otolith chemistry does not just reflect environmental conditions: A meta-analytic evaluation. *Fish Fisheries.* 19, 441–454. doi: 10.1111/faf.2018.19.issue-3

Kato, Y., Fujinaga, K., Nakamura, K., Takaya, Y., Kitamura, K., Ohta, J., et al. (2011). Deep-sea mud in the Pacific Ocean as a potential resource for rare-earth elements. *Nat. geoscience.* 4, 535–539. doi: 10.1038/ngeo1185

Kon, Y., Hoshino, M., Sanematsu, K., Morita, S., Tsunematsu, M., Okamoto, N., et al. (2014). Geochemical characteristics of apatite in heavy REE-rich deep-sea mud from minami-torishima area, southeastern Japan. *Resource Geology.* 64, 47–57. doi: 10.1111/rge.2014.64.issue-1

Li, D., Peng, J., Chew, D., Liang, Y., Hollings, P., Fu, Y., et al. (2023). Dating rare earth element enrichment in deep-sea sediments using U-Pb geochronology of bioapatite. *Geology* 51, 428–433. doi: 10.1130/G50938.1

Li, P., Shi, W., Liu, Q., Yu, Y., He, G., Chen, L., et al. (2011). Spatial and temporal distribution patterns of chlorophyll-a and the correlation analysis with environmental factors in Lake Qiandao. *J. Lake Sci. (in Chinese).* 23, 568–574. doi: 10.18307/2011.0412

Li, C., Zhou, L., Zhao, Z., Zhang, Z., Zhao, H., Li, X., et al. (2018). *In-situ* Sr isotopic measurement of scheelite using fs-LA-MC-ICPMS. *J. Asian Earth Sci.* 160, 38–47. doi: 10.1016/j.jseaes.2018.03.025

Liao, J., Chen, J., Sun, X., Wu, Z., Deng, Y., Shi, X., et al. (2022). Quantifying the controlling mineral phases of rare-earth elements in deep-sea pelagic sediments. *Chem. Geology.* 595, 120792. doi: 10.1016/j.chemgeo.2022.120792

Liao, J., Sun, X., Li, D., Sa, R., Lu, Y., Lin, Z., et al. (2019a). New insights into nanostructure and geochemistry of bioapatite in REE-rich deep-sea sediments: LA-ICP-MS, TEM, and Z-contrast imaging studies. *Chem. Geology.* 512, 58–68. doi: 10.1016/j.chemgeo.2019.02.039

Liao, J., Sun, X., Wu, Z., Sa, R., Guan, Y., Lu, Y., et al. (2019b). Fe-Mn (oxyhydr) oxides as an indicator of REY enrichment in deep-sea sediments from the central North Pacific. *Ore Geology Rev.* 112, 103044. doi: 10.1016/j.oregeorev.2019.103044

Ling, H., Jiang, S., Frank, M., Zhou, H., Zhou, F., Lu, Z., et al. (2005). Differing controls over the Cenozoic Pb and Nd isotope evolution of deepwater in the central North Pacific Ocean. *Earth Planetary Sci. Letters.* 232, 345–361. doi: 10.1016/j.epsl.2004.12.009

Liu, Z., Chen, Y., Ding, J., Zhang, W., Wu, Y., and Guo, F. (2003). Study on zoned characteristics and formation cause of the East China Sea submarine topography. *Adv. Mar. Science.* 21, 160–173.

Liu, Y., Jing, Y., and Zhao, W. (2023). Distribution of rare earth elements and implication for Ce anomalies in the clay-sized minerals of deep-sea sediment, Western Pacific Ocean. *Appl. Clay Science.* 235, 106876. doi: 10.1016/j.clay.2023.106876

Liu, J., Xu, H., Jiang, Y., Wang, J., and He, J. (2020). Mesozoic and Cenozoic shelf structure and tectonic evolution in the East China Sea Basin. *Acta Petrologica Sin. (in Chinese).* 94, 675–691. doi: 10.19762/j.cnki.dizhixuebao.2020115

Lu, Y., Zhang, X., Zhu, K., Wang, J., Yu, M., Huang, M., et al. (2022). Occurrence characteristics of rare earth elements in core sediments of the Central Indian Ocean Basin. *J. Rare Earths (in Chinese).* 41, 1006–1021.

Luo, C., Zheng, H., Tada, R., Wu, W., Irino, T., Yang, S., et al. (2014). Tracing Sr isotopic composition in space and time across the Yangtze River basin. *Chem. Geology.* 388, 59–70. doi: 10.1016/j.chemgeo.2014.09.007

Martin, E., and Haley, B. (2000). Fossil fish teeth as proxies for seawater Sr and Nd isotopes. *Geochimica Cosmochimica Acta* 64, 835–847. doi: 10.1016/S0016-7037(99)00376-2

Martin, E. E., and Scher, H. D. (2004). Preservation of seawater Sr and Nd isotopes in fossil fish teeth: bad news and good news. *Earth Planetary Sci. Letters.* 220, 25–39. doi: 10.1016/S0012-821X(04)00030-5

Martin, E. E., and Scher, H. (2006). A Nd isotopic study of southern sourced waters and indonesian throughflow at intermediate depths in the Cenozoic Indian Ocean. *Geochemistry Geophysics Geosystems* 7 (9). doi: 10.1029/2006GC001302

McArthur, J. M., Howarth, R. J., and Bailey, T. R. (2001). Strontium isotope stratigraphy: LOWESS version 3: best fit to the marine Sr-isotope curve for 0–509 Ma and accompanying look-up table for deriving numerical age. *J. Geology.* 109, 155–170. doi: 10.1086/319243

McArthur, J. M., Howarth, R. J., Shields, G. A., and Zhou, Y. (2020). Chapter 7 - Strontium isotope stratigraphy. *Geologic time scale* 1, 211–238.

Mi, B., Liu, S., Dou, Y., and Shi, X. (2017). Sr-Nd-Pb isotopic compositions in the sediments of the middle and small rivers around the East China Sea and the implications for tracing sediment sources. *Mar. Sci. Bull. (in Chinese).* 36, 440–448.

Mukhopadhyay, R. (1998). Post-Cretaceous intraplate volcanism in the central Indian Ocean Basin. *Mar. geology.* 151, 135–142. doi: 10.1016/S0025-3227(98)00073-5

Mukhopadhyay, R., George, P., and Ranade, G. R. (1997). Spreading rate dependent seafloor deformation in response to India-Eurasia collision: results of a hydrosweep survey in the Central Indian Ocean Basin. *Mar. geology.* 140, 219–229. doi: 10.1016/S0025-3227(97)00024-8

Nambiar, R., Bhushan, R., and Raj, H. (2022). Paleoredox conditions of bottom water in the northern Indian Ocean since 39 ka. *Palaeogeography Palaeoclimatology Palaeoecology.* 586, 110766. doi: 10.1016/j.palaeo.2021.110766

Nassar, N. T., Du, X., and Graedel, T. E. (2015). Criticality of the rare earth elements. *J. Ind. Ecol.* 19, 1044–1054. doi: 10.1111/jiec.2015.19.issue-6

Nemliher, J. G., Baturin, G. N., Kallaste, T. E., and Murdmaa, I. O. (2004). Transformation of hydroxyapatite of bone phosphate from the ocean bottom during fossilization. *Lithology Mineral Resources.* 39, 468–479. doi: 10.1023/B:LIMI.0000040736.62014.2d

Nozaki, Y., and Alibo, D. S. (2003). Importance of vertical geochemical processes in controlling the oceanic profiles of dissolved rare earth elements in the northeastern Indian Ocean. *Earth Planetary Sci. Letters.* 205, 155–172. doi: 10.1016/S0012-821X(02)01027-0

Ohta, J., Yasukawa, K., Nakamura, K., Fujinaga, K., Iijima, K., and Kato, Y. (2021). Geological features and resource potential of deep-sea mud highly enriched in rare-earth elements in the Central Pacific Basin and the Penrhyn Basin. *Ore Geology Rev.* 139, 104440. doi: 10.1016/j.oregeorev.2021.104440

Palmer, M. R., and Edmond, J. M. (1989). The strontium isotope budget of the modern ocean. *Earth Planetary Sci. Letters.* 92, 11–26. doi: 10.1016/0012-821X(89)90017-4

Pan, Y., and Fleet, M. E. (2002). Compositions of the apatite-group minerals: substitution mechanisms and controlling factors. *Rev. mineralogy geochemistry.* 48, 13–49. doi: 10.2138/rmg.2002.48.2

Pan, G., Xiao, Q., Lu, S., Deng, J., Feng, Y., Zhang, K., et al. (2009). Subdivision tectonic units of China. *Geology China (in Chinese).* 36, 1–28.

Paton, C., Hellstrom, J., Paul, B., Woodhead, J., and Hergt, J. (2011). Iolite: FREEware for the visualisation and processing of mass spectrometric data. *J. Analytical Atomic Spectrometry.* 26, 2508–2518. doi: 10.1039/c1ja10172b

Piotrowski, A. M., Banakar, V. K., Scrivner, A. E., Elderfield, H., Galy, A., and Dennis, A. (2009). Indian Ocean circulation and productivity during the last glacial cycle. *Earth Planetary Sci. Letters.* 285, 179–189. doi: 10.1016/j.epsl.2009.06.007

Piper, D. Z. (1974). Rare earth elements in the sedimentary cycle: a summary. *Chem. geology.* 14, 285–304. doi: 10.1016/0009-2541(74)90066-7

Rajendran, S., and Rao, T. P. (2000). Analysis of a north-south magnetic profile over the Central Indian Ocean. *Curr. Sci.* 78, 1378–1381. Available online at: https://www.jstor.org/stable/24104048.

Raju, K. K., and Ramprasad, T. (1989). Magnetic lineations in the Central Indian Basin for the period A24–A21: a study in relation to the Indian Ocean Triple Junction trace. *Earth Planetary Sci. Letters.* 95, 395–402. doi: 10.1016/0012-821X(89)90113-1

Ren, J., Jiang, X., He, G., Wang, F., Yang, T., Luo, S., et al. (2022). Enrichment and sources of REY in phosphate fractions: Constraints from the leaching of REY-rich deep-sea sediments. *Geochimica Cosmochimica Acta* 335, 155–168. doi: 10.1016/j.gca.2022.08.035

Ren, J., Liu, Y., Wang, F., He, G., Deng, X., Wei, Z., et al. (2021). Mechanism and influencing factors of REY enrichment in deep-sea sediments. *Minerals* 11, 196. doi: 10.3390/min11020196

Sa, R., Sun, X., He, G., Xu, L., Pan, Q., Liao, J., et al. (2018). Enrichment of rare earth elements in siliceous sediments under slow deposition: A case study of the central North Pacific. *Ore Geology Rev.* 94, 12–23. doi: 10.1016/j.oregeorev.2018.01.019

Scher, H. D., and Martin, E. E. (2006). Timing and climatic consequences of the opening of drake passage. *Science* 312, 428–430. doi: 10.1126/science.1120044

Shaw, H. F., and Wasserburg, G. J. (1985). Sm-Nd in marine carbonates and phosphates: Implications for Nd isotopes in seawater and crustal ages. *Geochimica Cosmochimica Acta* 49, 503–518. doi: 10.1016/0016-7037(85)90042-0

Sholkovitz, E. R. (1993). The geochemistry of rare earth elements in the Amazon River estuary. *Geochimica Cosmochimica Acta* 57, 2181–2190. doi: 10.1016/0016-7037(93)90559-F

Staudigel, H., Doyle, P., and Zindler, A. (1985). and Nd isotope systematics in fish teeth. *Earth Planetary Sci. Letters.* 76, 45–56. doi: 10.1016/0012-821X(85)90147-5

Su, J. (1998). Circulation dynamics of the China Seas north of 18° N. *sea.* 11, 483–505.

Subha Anand, S., Rahaman, W., Lathika, N., Thamban, M., Patil, S., and Mohan, R. (2019). Trace elements and Sr, Nd isotope compositions of surface sediments in the Indian Ocean: an evaluation of sources and processes for sediment transport and dispersal. *Geochemistry Geophysics Geosystems.* 20, 3090–3112. doi: 10.1029/2019GC008332

Sun, X., Fan, D., Liu, P., Pang, Y., and Tian, Y. (2017). The states of Eh, Ph of water from Yangtze River Estuary and its adjacent areas and their implications. *Adv. Mar. Sci. (in Chinese).* 35, 96–106.

Sun, X., Hu, Z., Liu, M., Pang, Y., and Fan., D. (2019). Distributions and influence factors of Eh and pH in the East China Sea in autumn. *Mar. Environ. Sci. (in Chinese).* 38, 211–220.

Sun, Z., Liu, J., Zhang, Y., Song, J., Xiao, Y., Yuan, H., et al. (2023). Compositional characteristics of sediment from Jiaozhou Bay in North China and the implication to the provenance. *J. Oceanology Limnology* 41, 1–13. doi: 10.1007/s00343-022-2019-z

Sun, Y., Shi, X., Yan, Q., Liu, X., Yu, M., Huang, M., et al. (2022). The study on geochemical characteristics and enrichment mechanism of deep sea REY-rich sediments in the Central Indian Ocean Basin. *Acta Oceanologica Sin. (in Chinese).* 44, 42–62.

Tanaka, E., Nakamura, K., Yasukawa, K., Mimura, K., Fujinaga, K., Iijima, K., et al. (2020). Chemostratigraphy of deep-sea sediments in the western North Pacific Ocean: Implications for genesis of mud highly enriched in rare-earth elements and yttrium. *Ore Geology Rev.* 119, 103392. doi: 10.1016/j.oregeorev.2020.103392

Tang, Z., Zhang, X., Zhang, M., Zhou, M., Tian, F., Wang, S., et al. (2023). Geochemical characteristics of soil elements in Xin'an River Basin: constrains from rock formation types. *East China Geology (in Chinese).* 44, 172–185.

Taylor, S. R., and McLennan, S. M. (1985). *The continental crust: its composition and evolution.* (Oxford: Blackwell Scientific Publications).

Toyoda, K., and Tokonami, M. (1990). Diffusion of rare-earth elements in fish teeth from deep-sea sediments. *Nature* 345, 607–609. doi: 10.1038/345607a0

Trueman, C. N. G., Behrensmeyer, A. K., Tuross, N., and Weiner, S. (2004). Mineralogical and compositional changes in bones exposed on soil surfaces in Amboseli National Park, Kenya: Diagenetic mechanisms and the role of sediment pore fluids. *J. Archaeological Science.* 31, 721–739. doi: 10.1016/j.jas.2003.11.003

Tütken, T., Vennemann, T. W., and Pfretzschner, H. U. (2008). Early diagenesis of bone and tooth apatite in fluvial and marine settings: Constraints from combined oxygen isotope nitrogen and REE analysis. *Palaeogeography Palaeoclimatology Palaeoecology.* 266, 254–268. doi: 10.1016/j.palaeo.2008.03.037

Vanderstraeten, A., Mattielli, N., Laruelle, G. G., Gili, S., Bory, A., Gabrielli, P., et al. (2023). Identifying the provenance and quantifying the contribution of dust sources in EPICA Dronning Maud Land ice core (Antarctica) over the last deglaciation (7–27 kyr BP): A high-resolution, quantitative record from a new Rare Earth Element mixing model. *Sci. Total Environment.* 881, 163450. doi: 10.1016/j.scitotenv.2023.163450

Wang, T., Dong, Y., Chu, F., Zhang, W., Li, X., Su, R., et al. (2023). *In situ* Strontium isotope stratigraphy of fish teeth in deep-sea sediments from the western Clarion-Clipperton Fracture Zone, eastern Pacific Ocean. *Chem. Geology.* 636, 121624. doi: 10.1016/j.chemgeo.2023.121624

Wang, F., He, G., Sun, X., Yang, Y., and Zhao, T. (2016). Study on rare earth elements occurrence carriers in REY-rich deep-sea sediments in the Pacific Ocean. *Acta Petrologica Sin. (in Chinese).* 32, 2057–2068.

Wei, Q., Wang, B., Chen, J., Xia, C., Qu, D., and Xie, L. (2015). Recognition on the forming-vanishing process and underlying mechanisms of the hypoxia off the Yangtze River estuary. *Sci. China Earth Sci.* 58, 628–648. doi: 10.1007/s11430-014-5007-0

Weng, B. S., Wan, R. A., Yu, R. L., Hu, G. R., Yan, Y., Lin, C. Q., et al. (2023). Characteristics and provenances of rare earth elements and Nd isotopes in surface sediments of mangrove wetlands in the Jiulong River Estuary, China. *Environ. Sci. pollut. Res.* 30, 73890–73898. doi: 10.1007/s11356-023-27558-1

Wright, J., Schrader, H., and Holser, W. T. (1987). Paleoredox variations in ancient oceans recorded by rare earth elements in fossil apatite. *Geochimica Cosmochimica Acta* 51, 631–644. doi: 10.1016/0016-7037(87)90075-5

Wright, J., Seymour, R. S., and Shaw, H. F. (1984). REE and Nd isotopes in conodont apatite: variations with geological age and depositional environment. *Conodont biofacies provincialism.* 196, 325–340. doi: 10.1130/SPE196

Yang, Y., Wu, F., Yang, J., Chew, D., Xie, L., Chu, Z., et al. (2014). and Nd isotopic compositions of apatite reference materials used in U–Th–Pb geochronology. *Chem. Geology.* 385, 35–55. doi: 10.1016/j.chemgeo.2014.07.012

Yasukawa, K., Liu, H., Fujinaga, K., Machida, S., Haraguchi, S., Ishii, T., et al. (2014). Geochemistry and mineralogy of REY-rich mud in the eastern Indian Ocean. *J. Asian Earth Sci.* 93, 25–36. doi: 10.1016/j.jseaes.2014.07.005

Zeng, J., Long, S., Bao, M., Li, Y., and Li, Y. (2012). Analysis of dominant ingredients and trace elements of offshore sea water in Yangshan, Shanghai. *Mar. Environ. Sci. (in Chinese)* 31, 186–189+200.

Zhang, X., Lu, Y., Miao, Y., Huang, M., Zhu, K., Cai, L., et al. (2023). Radiogenic Nd in bioapatite from rare earth elements rich deep sea sediments from Central Indian Oceanic Basin and its implication in material sources. *Ore Geology Rev.* 154, 105295. doi: 10.1016/j.oregeorev.2023.105295

Zhang, X., Tao, C., Shi, X., Li, H., Huang, M., and Huang, D. (2017). Geochemical characteristics of REY-rich pelagic sediments from the GC02 in central Indian Ocean Basin. *J. Rare Earths* 35, 1047–1058. doi: 10.1016/S1002-0721(17)61012-3

Zhao, L., Chen, Z. Q., Algeo, T. J., Chen, J., Chen, Y., Tong, J., et al. (2013). Rare-earth element patterns in conodont albid crowns: evidence for massive inputs of volcanic ash during the latest Permian biocrisis? *Global Planetary Change.* 105, 135–151. doi: 10.1016/j.gloplacha.2012.09.001

Zhou, X., Yan, X., and Sun, W. (2015). Some numerical simulations of circulation in the east China sea. *Appl. Mechanics Materials.* 733, 427–430. doi: 10.4028/www.scientific.net/AMM.733